FAST AND THERMAL NEUTRON FLUXES IN A GRAPHITE MODERATOR

by

Ralph Richard Hedges

A Thesis Submitted to the
Graduate Faculty in Partial Fulfillment of
The Requirements for the Degree of
MASTER OF SCIENCE

Major Subject: Nuclear Engineering

Iowa State College
Ames, Iowa
1959

TABLE OF CONTENTS

TABLE OF CONTENTS (Continued)

INTRODUCTION

The natural uranium, graphite moderated subcritical assembly constructed at Iowa State College has been utilized for several theses investigations by graduate students. A large number of the operating characteristics have been investigated, but a review of the theses disclosed that a determination of the actual neutron flux throughout the assembly had not been undertaken.

The purpose of this thesis was to obtain the fast and thermal neutron fluxes throughout the assembly with the fuel removed. In addition, the thermal neutron source which was equivalent to the existing fast source was to be calculated.

This assembly, with the fuel removed, consisted of a rectangular parallelpiped of graphite moderator with an external fast neutron source. This moderating system is essentially a "sigma pile" with holes interspersed at regular intervals.

REVIEW OF LITERATURE

A development of the theoretical thermal and fast neutron flux distribution in a system consisting of a graphite moderator and a fast neutron source was presented in Glasstone and Edlund (8). The theory underlying the treatment of fast neutrons as a single group was developed by Hughes (12).

The various research techniques that have been developed for measuring fast and thermal fluxes were discussed at length by Hughes (12). The procedures used to measure flux, and calibrate the subcritical assemblies and moderators at the Argonne National Laboratory were covered in detail by Hoag (11).

The induced beta activity of indium foils has been used frequently to evaluate neutron fluxes. A commonly used method of obtaining neutron fluxes appeared to be the use of a combination of indium foils and a calibrated counter. The preparation of a standard source and the utilization of the source to calibrate the counter was presented by Bleuler and Goldsmith (2).

Considerable insight into the field of activation calibration was obtained from the reports of the Atomic Energy Commission laboratories which have published the results of their research. In 1951 the procedures used and the results obtained from the calibration of the Hanford Standard Pile

were released by the Atomic Energy Commission (4). Indium foils were used for flux measurements and for calibrating the counters. The absolute neutron fluxes were measured in the Hanford Standard Pile in 1954 (5). These measurements were obtained by activation techniques using gold and indium foils. The X-10 standard graphite pile of the Oak Ridge National Laboratory was calibrated in 1952 (14). The flux measurements were obtained by gold foil activation.

In a series of three reports released between 1955 and 1957, the nuclear engineering department of North American Aviation described the methods used in their laboratory to determine absolute thermal neutron flux. The first report presented the methods used to determine the ratio of thermal to resonance neutron densities using indium foils (9). Their second report described the procedure used for absolute beta counting (15). The final report of the series explained the technique of obtaining absolute thermal neutron fluxes using activated indium foils (10).

Information regarding the physical and operating properties of the graphite moderator described herein was obtained from the research of previous graduate students at Iowa State College who conducted various experiments on the subcritical assembly.

LIST OF SYMBOLS

Symbol	Units	Meaning
A	gm./gm. atomic wt.	Atomic weight
A_{mn}	neutrons/in.^{2} sec. neutrons/cm.^{2} sec.	Composite source constant
A_∞	cpm., cps.	Actual saturation activity
a	in.	Distance along x axis between zero flux positions
b	in.	Distance along y axis between zero flux positions
C	neutrons/in.^{2} sec. neutrons/cm.^{2} sec.	Proportionality constant
C_e		End correction factor
C_h		Harmonic correction factor
C_v		Coefficient of variation
c	in.	Distance along z axis from source to zero flux position
D	in., cm.	Diffusion coefficient
$d_{\frac{1}{2}}$	mg./cm.^{2}	Half thickness
E	ev.	Energy
f_b		Back scattering factor
f_c		Gamma correction factor
f_e		Efficiency factor
f_g		Geometry factor
f_s		Self absorption factor
f_t		Total correction factor

Symbol	Units	Meaning
f_w		Absorption factor
f_1		$(f_g)\cdot(f_b)\cdot(f_e)$
f_τ		Dead time factor
I		Number of logarithmic increments
In		Indium
In^{115}		Indium isotope
J_{mn}	neutrons/in.^{2} sec. neutrons/cm.^{2} sec.	Neutron current density due to mode m, n
m	cpm., cps.	Measured saturation activity
m_w	cpm./gm.	Measured normalized saturation activity
N	neutrons/cm.^{3}	Neutrons per unit volume
N_a	atoms/gm. atomic wt.	Avagadroes number
q	neutrons/in.^{3} sec. neutrons/cm.^{3} sec.	Slowing down density
S	neutrons/sec.	Equivalent thermal neutron source strength due to the first mode only
S_{mn}	neutrons/sec.	Thermal neutron source strength due to mode m, n
t	mg./cm.^{2}	Thickness
V	in.^{3}, cm.^{3}	Volume
v	cm./sec.	Velocity
W	gm., mg.	Weight
x	in., cm.	Distance along horizontal axis representing depth of moderator
y	in., cm.	Distance along horizontal axis representing width of moderator

Symbol	Units	Meaning
z	in., cm.	Distance along vertical axis representing height of moderator
β		Beta particle
γ	$in.^{-1}$, $cm.^{-1}$	Inverse relaxation length, subscripts denote mode
γ_{mn}	$in.^{-1}$, $cm.^{-1}$	Inverse relaxation length due to mode m, n
γ_{11}	$in.^{-1}$, $cm.^{-1}$	Inverse relaxation length due to first mode only
Δ		Increment
$\delta(x,y)$		Dirac delta function
χ	$in.^{-1}$, $cm.^{-1}$	Inverse diffusion length
λ_t	in., cm.	Transport mean free path
μ_a	$cm.^2/mg.$	Absorption coefficient
ξ		Logarithmic energy decrement
ρ	$gm./cm.^3$ $mg./cm.^3$	Density
Σ		Summation
Σ_a	$cm.^{-1}$	Macroscopic activation cross section
σ		Standard deviation
σ_a	$cm.^2$	Microscopic absorption cross section
σ_{act}	$cm.^2$	Microscopic activation cross section
σ_s	$cm.^2$	Microscopic scattering cross section

Symbol	Units	Meaning
Φ	neutrons/cm.^{2} sec.	Thermal neutron flux
Φ_f	neutrons/cm.^{2} sec.	Fast neutron flux
Φ_{mn}	neutrons/cm.^{2} sec.	Thermal neutron flux due to mode m, n
Φ_{11}	neutrons/cm.^{2} sec.	Thermal neutron flux due to first mode only
∇		Laplacian operator

THEORETICAL NEUTRON FLUXES

Thermal Flux

General

Consider a rectangular parallelpiped of moderator material with a plutonium - beryllium source at one end. The source is a point source of fast neutrons. However, after the neutrons have passed through a short distance in the moderator a large portion of the fast neutrons will be thermalized. These thermal neutrons are essentially monoenergetic, so it is possible to postulate a distributed plane source of monoenergetic neutrons at the base of the parallelpiped, $z = 0$.

Determination of flux distribution in this moderator is effected by solving the wave equation for positive values of z away from the source and all physical boundaries (8, p. 118).

$$\nabla^2 \phi - \varkappa^2 \phi = 0, \qquad \text{Eq. 1}$$

where ∇^2 is the Laplacian operator, ϕ is the thermal neutron flux, and $\varkappa$ is the reciprocal of the diffusion length.

Boundary conditions necessary to solve this equation are:

(a) The flux is everywhere finite and non negative.

(b) The x and y dimensions of the block are a and b

respectively. These distances are the lengths along the respective axes between points of zero flux on the z = 0 plane. Effectively these are equivalent to the distance between the physical boundaries plus the extropolated distances. The distance c is the distance along the z axis from z = 0 to where the flux is zero.

(c) The source condition will be considered when it is applied to the solution.

Eq. 1 expressed in rectangular coordinates is

$$\frac{\partial^2 \phi}{\partial x^2} + \frac{\partial^2 \phi}{\partial y^2} + \frac{\partial^2 \phi}{\partial z^2} - \kappa^2 \phi = 0. \qquad \text{Eq. 2}$$

Applying boundary conditions (a) and (b), the following solution is obtained for Eq. 2 (8, p. 121):

$$\phi = \sum_{m=1}^{\infty} \sum_{n=1}^{\infty} A_{mn} \left[\cos \frac{m\pi x}{a} \cos \frac{n\pi y}{b} e^{-\gamma_{mn} z} \right] \left[1 - e^{-2\gamma_{mn}(c-z)} \right] \qquad \text{Eq. 3}$$

The quantity γ_{mn} is defined as

$$\gamma_{mn}^2 = \left(\frac{m\pi}{a}\right)^2 + \left(\frac{n\pi}{b}\right)^2 + \kappa^2. \qquad \text{Eq. 4}$$

The quantity A_{mn}, a combination of all the constants obtained in the development of Eq. 3, must be evaluated with the source condition.

The source condition to be satisfied, boundary condition (c), is that the number of neutrons flowing out of the plane z = 0 per unit area per second for the mn mode must equal the number produced by the source in that mode. To satisfy boundary condition (c) the net current density, J_{mn}, is evaluated as follows (8, p. 121):

$$J_{mn} = -D \left(\frac{\partial \phi_{mn}}{\partial z}\right)_0 = \left(D \gamma_{mn} A_{mn} \cos \frac{m \pi x}{a} \cos \frac{n \pi y}{b}\right) \left(e^{-\gamma_{mn} z}\right). \qquad \text{Eq. 5}$$

A source of this type may be written as $S\,\delta(x,y)$ at z = 0, where $\delta(x,y)$ is the Dirac delta function. From the definition of the Dirac delta function, the value of the source, S, at the origin, x = y = z = 0, is

$$S = S(0) = \int_{-\infty}^{+\infty} S(x)\,\delta(x)\,dx. \qquad \text{Eq. 6}$$

Eq. 6 is expanded in a series of orthogonal functions which satisfy the boundary conditions (8, p. 122). Eq. 6 becomes

$$S\,\delta(x,y) = \sum_{m=1}^{\infty} \sum_{n=1}^{\infty} S_{mn} \cos \frac{m \pi x}{a} \sin \frac{n \pi y}{b}. \qquad \text{Eq. 7}$$

$$S_{mn} = \frac{4 S}{a b}. \qquad \text{Eq. 8}$$

Since S in Eq. 7 and 8 represents the neutrons emitted in the +z and -z directions, the equivalent source for the moderator in the +z direction is

$$S_{mn} = \frac{2S}{a\,b}. \qquad \text{Eq. 9}$$

Comparison of Eq. 5 and 7 gives the following value for A_{mn}:

$$A_{mn} = \frac{2S}{a\,b\,D\,\gamma_{mn}}. \qquad \text{Eq. 10}$$

The source term, S, is the number of thermal neutrons emitted per second by a point source located at x = y = z = 0. The constant D is the moderator diffusion coefficient for flux; it has the dimensions of length. The equation for the flux, Eq. 3, now becomes

$$\phi = \frac{2S}{a\,b\,D} \sum_{m=1}^{\infty} \sum_{n=1}^{\infty} \frac{e^{-\gamma_{mn} z}}{\gamma_{mn}} \cos \frac{m\pi x}{a} \cos \frac{n\pi y}{b}$$

$$\left[1 - e^{-2\gamma_{mn}(c-z)} \right]. \qquad \text{Eq. 11}$$

Limit the expansion of Eq. 11 to the first and third modes, and Eq. 11 becomes

$$\phi = \frac{2S}{a\,b\,D} \frac{e^{-\gamma_{11} z}}{\gamma_{11}} \cos \frac{\pi x}{a} \cos \frac{\pi y}{b}$$

$$\left\{ 1 + \frac{\gamma_{11}\, e^{\gamma_{11} z}}{\cos \frac{\pi x}{a} \cos \frac{\pi y}{b}} \left(\frac{e^{-\gamma_{13} z}}{\gamma_{13}} \cos \frac{\pi x}{a} \cos \frac{3\pi y}{b} + \frac{e^{-\gamma_{31} z}}{\gamma_{31}} \cos \frac{3\pi x}{a} \cos \frac{\pi y}{b} \right. \right.$$

$$+ \frac{e^{-\gamma_{33} z}}{\gamma_{33}} \cos \frac{3\pi x}{a} \cos \frac{3\pi y}{b} \Bigg) \Bigg\}$$

$$\left[1 - e^{-2\gamma_{11}(c-z)} \right]. \qquad \text{Eq. 12}$$

The terms included in the braces in Eq. 12 make up the harmonic correction term, C_h. The terms included in the brackets make up the end correction term, C_e. With these substitutions Eq. 12 can be written as

$$\phi = \frac{2S}{a\,b\,D} \frac{e^{-\gamma_{11} z}}{\gamma_{11}} \cos \frac{\pi x}{a} \cos \frac{\pi y}{b} (C_h)(C_e). \qquad \text{Eq. 13}$$

The thermal neutron flux due to the first mode only, ϕ_{11}, is obtained as follows:

$$\phi_{11} = \frac{\phi_{mn}}{(C_h)(C_e)} = C\, e^{-\gamma_{11} z} \cos \frac{\pi x}{a} \cos \frac{\pi y}{b}, \qquad \text{Eq. 14}$$

where

$$C = \frac{2S}{a\,b\,D\gamma_{11}}.$$

Activation

Consider a particular element which forms a radioisotope when it absorbs a neutron. The amount of this radioisotope formed can be determined by measuring its radioactivity. If a thin foil of this element is exposed to a neutron flux for sufficient time to become saturated with radiation, the measured activity of this foil is its saturation activity, A_∞.

If the foil is thin, the neutron density may be regarded as constant throughout the foil because the foil does not depress the neutron flux significantly. If the volume, V, and the macroscopic activation cross section, Σ_a, of the foil are known, the flux can be determined as follows (8, p. 53):

$$\phi = \frac{A_\infty}{(V)(\Sigma_a)} . \qquad \text{Eq. 15}$$

Since Σ_a varies with the energy of neutrons, Eq. 15 applies only to monoenergetic neutrons. Thermal neutrons are considered monoenergetic, so Eq. 15 can be used to calculate thermal neutron flux.

Fast Flux

General

Consider a rectangular parallelpiped of moderator material with a plutonium-beryllium source at one end. The source is considered a point source with a known energy spectrum. The moderator consists of a material which has a low absorption cross section as well as a high slowing down power.

Assume the absorption of neutrons in the moderator is negligible, then the distribution in energy of the neutrons while slowing down can be obtained as follows (12, p. 28): Assume q neutrons are produced per unit volume in the mod-

erator. The slowing down density, q (E), which is the number of neutrons passing a given energy per unit time per unit volume is

$$q(E) = n(E)\,\Delta E\, v\, N\, \sigma_s, \qquad \text{Eq. 16}$$

where n (E) is the density of neutrons per unit energy, ΔE is the energy loss per collision, v is the velocity of the neutron at the particular energy, N is the neutrons per unit volume within the energy interval, and σ_s is the scattering cross section of the moderator. Substitute ξ, the loss in ln. E per collision, and ΔE in Eq. 16 is equal to ξE. Substitute ξ, the neutron flux, for n v and the neutron flux per unit energy becomes $\phi(E)$. Then Eq. 16 becomes

$$q(E) = \phi(E)\, E\, \xi\, N\, \sigma_s. \qquad \text{Eq. 17}$$

For no absorption q (E) equals q, thus,

$$\phi(E) = \frac{q}{\xi N \sigma_s} \frac{1}{E}, \qquad \text{Eq. 18}$$

and the flux throughout the energy spectrum can be represented by

$$\phi(E)\, dE = \frac{q\, dE}{\xi \Sigma_s E}. \qquad \text{Eq. 19}$$

Therefore, the flux in the slowing down region is proportional to dE/E.

The flux within any energy increment can be evaluated as

$$\phi(E_2) - \phi(E_1) = \frac{q}{\xi \Sigma_s} \; 2.3 \log_{10} \left(\frac{E_2}{E_1}\right). \qquad \text{Eq. 20}$$

If the increments of energy are taken such that $E_2/E_1 = 10$, then

$$\Phi_2 - \Phi_1 = 2.3 \frac{q}{\xi \Sigma_s}, \qquad \text{Eq. 21}$$

and the fast neutron flux, Φ_f, is obtained from the summation of the flux in each energy interval over the energy spectrum.

$$\Phi_f = \sum_{\text{Spectrum}} \Delta\phi(E) = (I)\,(2.3) \frac{q}{\xi \Sigma_s}, \qquad \text{Eq. 22}$$

where I represents the number of intervals of E_2/E_1 included in the energy spectrum of the source.

Activation

The basic theory presented for the measurement of thermal neutron flux by activation holds true for the measurement of fast neutron flux. However, Eq. 15 must be modified to allow for the variation in activation cross section with energy. The saturated activity, A_∞, can be written in the form (8, p. 161),

$$A_\infty = V \int \Sigma_a (E)\; \phi(E)\; dE, \qquad \text{Eq. 23}$$

where Σ_a (E) is the macroscopic activation cross section of the foil for neutrons of energy E, and ϕ(E) is the neutron

flux per unit energy interval at this energy. Since the measurement is being made in a moderator in which the absorption of neutrons is small compared with the scattering, $\Phi(E)$ can be related to the slowing down density by (8, p. 160)

$$\Phi(E) = \frac{q}{\xi \Sigma_s E} \qquad \text{Eq. 24}$$

where ξ is the loss in ln. E per collision, and Σ_s is the macroscopic scattering cross section of the moderator which is assumed to be constant in a weakly absorbing moderator. Thus, Eq. 24 can be written as

$$A_\infty = \frac{q\,V}{\xi\,\Sigma_s} \int \Sigma_a (E)\, \frac{dE}{E} . \qquad \text{Eq. 25}$$

Eq. 25 can be rewritten in terms of the microscopic activation cross section, σ_{act}, as

$$A_\infty = \frac{q}{\xi\ \Sigma_s} (N\ V) \int \sigma_{act}\ (E)\ \frac{dE}{E} \qquad \text{Eq. 26}$$

where N is the number of neutrons per unit volume within the energy interval. To obtain the fast neutron flux, the activity must be measured over the energy interval from 0.4 ev. to the maximum energy of the source. The fast neutron flux is related to neutrons with energies above 0.4 ev.; whereas, the thermal neutron flux is related to neutrons below 0.4 ev. (11, p. 66). The constant, $q/\xi\ \Sigma_s$, can be evaluated from

Eq. 26; this constant substituted into Eq. 22 provides a means for determining the fast neutron flux.

EXPERIMENTAL EQUIPMENT

Moderator

The moderator utilized for this experimental work was the Iowa State College subcritical assembly with fuel removed shown in Figure 1. It consisted of rectangular blocks of graphite which had a specific weight of 97.3 pounds per cubic foot stacked 10 rows wide and 11 layers high. Each block was 60 inches long. The first nine layers of blocks were 6 in. wide and 6 in. high; the top five layers were 6 in. wide and 5 in. high. The graphite blocks were cut from 7 in. diameter cylindrical rods so that the rounded corners provided holes in the moderator into which fuel rods or measuring apparatus could be inserted. The overall dimensions of the moderator were 61 in. by 63.25 in. by 79 in.

The moderator was positioned on a wooden frame which rested on a concrete floor. The 12 inches between the concrete floor and the base of the moderating material permitted three open topped aluminum tanks to be inserted under the plywood upon which the moderating material rested. These tanks covered the base area of the moderator, and were kept full of water. A small compartment was constructed in the center of the middle tank to house the source.

The moderator was covered on the top and sides with a

Figure 1. The subcritical assembly

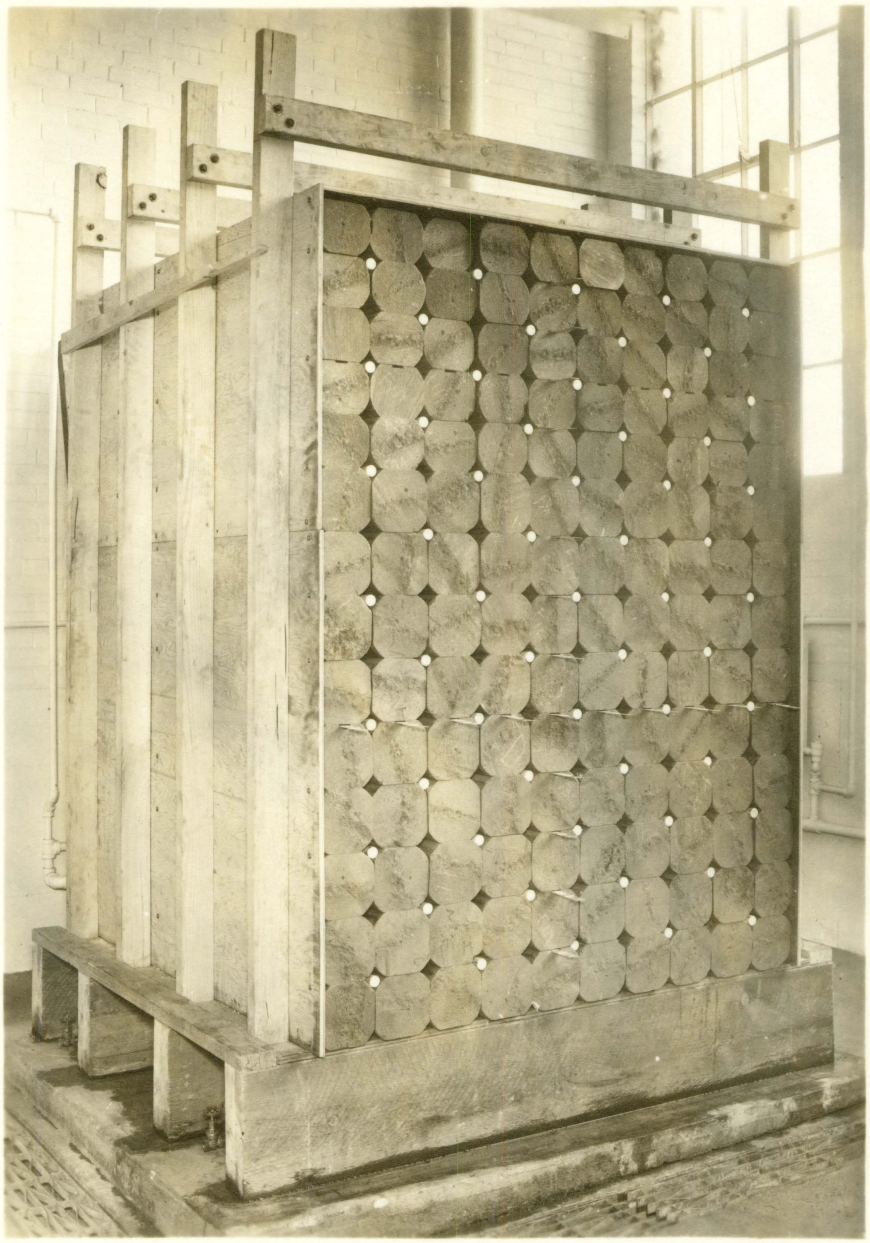

sandwich construction consisting of masonite, plywood, and a 0.010 inch cadmium sheet. The latter presented an effective "black boundary" to the neutrons.

Five separate plutonium-beryllium capsules, encased in tantalum and stainless steel cylinders, provided the neutron source. These cylinders were 1 in. in diameter and 1.375 in. high. Each source had an average rated strength of 1.63 x 10^6 neutrons per second. The sources were mounted upright in a wooden frame with the top of the cylinder 1/16 in. beneath the base of the moderator. The sources were positioned to form a cruciform oriented along the x and y axes of the moderator as shown in Figure 2.

Activation Foils

Indium foils were used to measure the neutron flux through foil activation. The foils were 0.003 in. by 1.0 in. by 1.5 in. and each was weighed to the nearest 0.1 mg. Each foil weighed approximately 0.59 grams. The foils were glued to aluminum planchets, which were taped to wooden yard sticks, which could be inserted into any of the holes throughout the moderator. The cadmium used to shield the indium foils from thermal neutron flux formed a package with an effective cadmium thickness of 0.020 in.

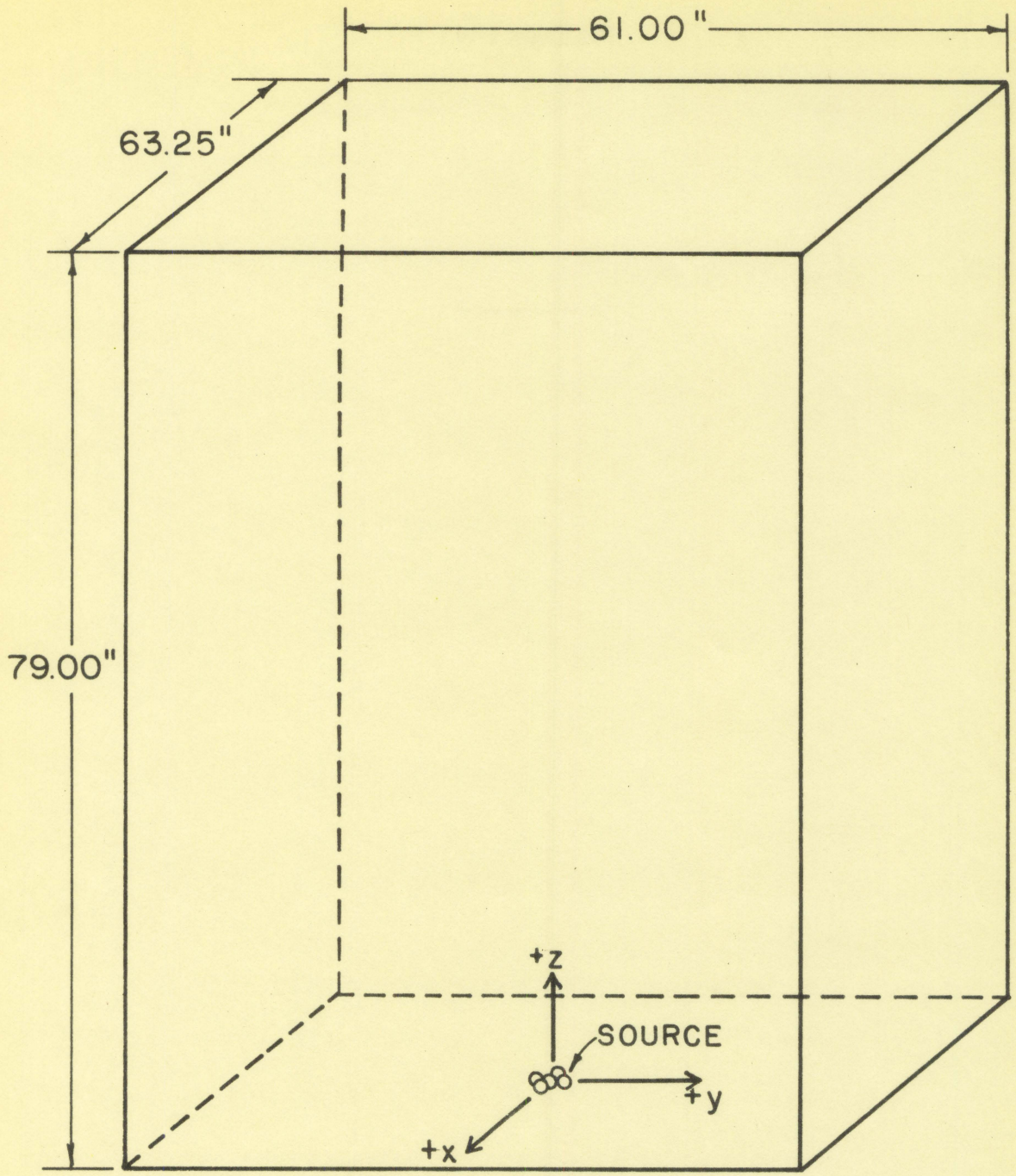

Figure 2. Graphite moderator

Counting Equipment

All indium foil activities were counted with a Nuclear Chicago end window Geiger-Müller tube. The end window was mica with a thickness of 1.4 mg. per cm^2. A Nuclear Chicago decade scaler was used in conjunction with the counter. The activated foils were placed 0.071 inches from the end window of the counter. The foils were positioned on an aluminum tray in a lead shield for counting.

EXPERIMENTAL PROCEDURE

Activation of Indium Foils

To determine the neutron flux distribution throughout the moderator it was necessary to measure the activity of irradiated indium foils periodically throughout just ¼ of the moderator. Since there was symmetry in the + and - directions along both the x and y axes (1, p. 40), measurements from the origin along the +x axis, the -y axis, and the +z axes, as shown in Figure 2, were adequate for coverage throughout the moderator. Foils were activated at x = 0, 10, and 20 in., y = 0, -6, -12, -18, -24 and -30 in. on a single plane of the z axis on each experimental run. Thirteen surveys were made with bare indium foils at z = 6, 12, 18, 24, 30, 36, 42, 48, 54, 59, 64, 69, and 74 in. Eight runs were made with cadmium covered indium foils at z = 6, 12, 18, 24, 30, 36, 42, and 48 in. The cadmium covered surveys were discontinued after eight runs because the activity at the upper levels could not be distinguished from the background.

The indium foils were irradiated for a minimum of eight hours. This insured an activity of 99.8 per cent saturation activity of the 54 minute half life, indium beta particle. The saturation activity represented the equilibrium condition in which the disintegration rate equaled the formation of

radioactive nuclei.

Measured activities of each foil were corrected for background. This activity was corrected to saturated activity at the time of removal from the moderator, and was then divided by the weight in grams of the particular foil to obtain a normalized saturation activity, m_w (11, p. 70-77), where m_w equaled counts per minute per gram of foil.

Determination of Actual Saturation Activity

To determine the neutron fluxes, it was necessary to convert the normalized saturation activity, m_w, to the actual saturation activity, A_∞. This was accomplished by calibrating the counter with a standard sample. The preparation of the standard sample, and the methods used to calibrate the counter were delineated in Appendix A. The total correction factor, f_t, for all the indium foils was determined to be 0.0454.

$$A_\infty = \frac{m_w}{(60)\, f_t} = \frac{m_w}{(60)\ (0.0454)} \frac{\text{counts}}{\text{sec}} . \qquad \text{Eq. 27}$$

Thermal Flux Determination

The actual saturation activity, A_∞, is the disintegration rate of the saturated indium foils. It is related to the thermal neutron flux, ϕ, as shown in Eq. 15.

$$A_\infty = V \Sigma_a \phi , \qquad \text{Eq. 15}$$

where

A_∞ = saturation activity, cps.

V = volume of foil, $cm.^3$

Σ_a = macroscopic activation cross section, $cm.^{-1}$

ϕ = thermal neutron flux, neutrons/$cm.^2$ sec.

Then Eq. 15 was rearranged,

$$m_w = \frac{60 \, V \, N \, \sigma_{act} \, \phi \, f_t}{W} \qquad \text{Eq. 28}$$

where

m_w = counts/min./gm. = $\frac{(A_\infty)(60)(f_t)}{W}$

W = normalized weight of foil, 1 gram,

f_t = correction factor,

N_a = Avagadroes number, $6.023(10)^{23}$ atoms/gm. atomic weight,

A = atomic weight of indium, 115 gm./gm. atomic weight,

$\frac{In^{115}}{In}$ = fraction by weight of In^{115} in In, 0.9577, and

σ_{act} = activation cross section of In^{115} for thermal neutrons, $155 \, (10)^{-24}$ $cm.^2$

The activation cross section of In^{115} was determined from the data compiled at the Brookhaven National laboratory (13).

The activation cross section was determined for the 54 minute half life β particle. The effect of the 13 second half life β particle was eliminated by waiting 2 minutes

before counting the activated foils. However, some gamma radiation did accompany the β decay (7, p. 426). To determine the actual amount of gamma radiation present, an absorption curve was obtained using several thicknesses of absorbers, and the curve was plotted in Figure 3. The gamma activity was extrapolated back to zero absorber to get the fraction of the total measured activity which was due to gamma radiation. The gamma correction factor, f_c, was determined to be 39/40 since 1/40 of the total activity was due to gamma activity. Eq. 28 was then expressed as

$$\Phi = \frac{m_w \; A \; (In) \; (f_c)}{60 \; (f_t) \; (\sigma_{act}) \; (N_a) \; (In^{115})} \qquad \text{Eq. 29}$$

$$= \frac{m_w \; 115}{(60) \; (0.0454) \; (155) \; (10)^{-24} \; (6.023) \; (10)^{23}} \; \frac{(39)}{(0.9577) \; (40)}$$

$$= \frac{m_w}{2.175} \; \frac{\text{neutrons}}{\text{cm.}^2 \; \text{sec.}} \; .$$

The values of the thermal neutron flux, Φ, throughout the moderator are tabulated in Table 1.

Fast Flux Determination

The effective fast neutron flux, Φ_f, was determined from Eq. 22.

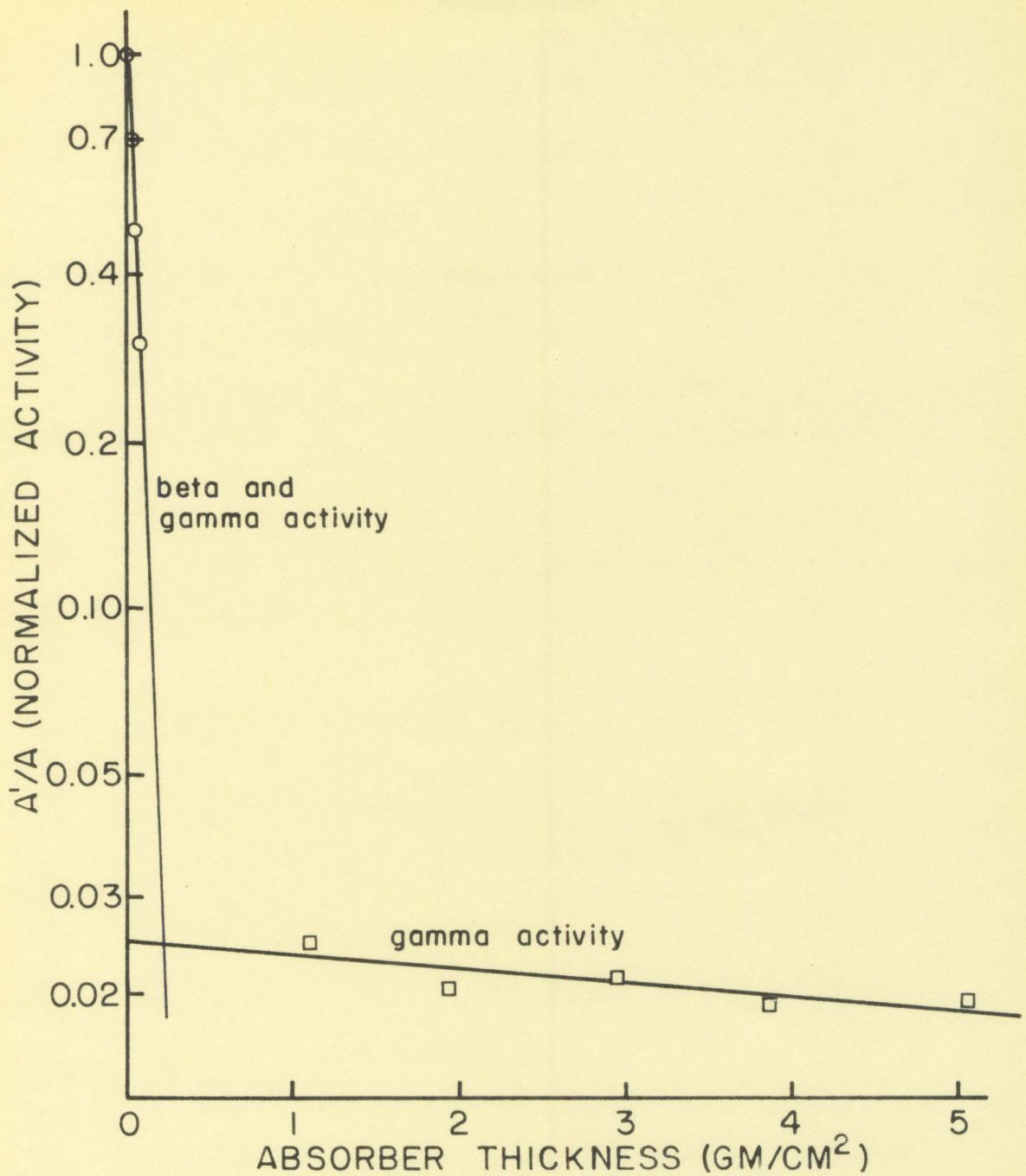

Figure 3. Determination of gamma activity

Table 1. Thermal neutron flux (neutrons/cm^2 sec.)

y, in.	0			-6			-12			-18			-24		
x, in.	0	10	20	0	10	20	0	10	20	0	10	20	0	10	20
z, in.															
6	2750	2098	960	2695	1880	867	2358	1458	724	1055	843	555	664	600	351
12	2240	1650	855	2010	1510	783	1519	1181	610	952	820	438	493	462	245
18	1521	1232	635	1381	1068	547	1160	971	444	728	622	348	405	332	182
24	994	815	431	904	747	414	724	577	359	520	423	255	297	250	125
30	648	520	292	580	475	295	488	450	232	335	294	162	185	171	86
36	390	335	194	373	300	181	297	252	157	256	194	117	131	112	69
42	225	202	113	208	188	110	204	171	88	109	93	72	65	64	47
48	121	114	63	97	91	60	95	84	51	72	59	35	54	40	29
54	70	68	36	68	58	33	67	45	22	28	23	18	23	21	15
59	47	43	31	46	39	30	38	35	19	27	21	15	21	16	14
64	41	36	22	34	36	22	31	28	17	25	12	10	12	10	9
69	29	25	19	24	21	17	18	17	10	17	16	13	15	10	10
74	19	18	7	13	11	11	13	12	9	11	10	8	11	11	8

$$\Phi_f = \sum_{\text{Spectrum}} \Delta\phi(E) = (I)\ (2.3)\ \frac{q}{\xi\ \Sigma_s} . \qquad \text{Eq. 22}$$

The energy spectrum of the plutonium-beryllium source extended from zero to 10.5 Mev. (16). The symbol I represented the number of intervals of E_2/E_1, extending over the source spectrum where E_2/E_1, equaled 10. The energy intervals are tabulated on Table 2, where I was determined to be 7.26.

Table 2. Energy intervals

Number of intervals		Energy limits, ev.		
1.00		0.4	to	4
1.00		4	to	$4(10)^1$
1.00		$4(10)^1$	to	$4(10)^2$
1.00		$4(10)^2$	to	$4(10)^3$
1.00		$4(10)^3$	to	$4(10)^4$
1.00		$4(10)^4$	to	$4(10)^5$
1.00		$4(10)^5$	to	$4(10)^6$
0.26		$4(10)^6$	to	$10.5(10)^6$
7.26	Total	0.4	to	$10.5(10)^6$

The quantity, $q/\xi\ \Sigma_s$, was evaluated from Eq. 26,

$$A_\infty = \frac{q}{\xi\ \Sigma_s}\ (N\ V) \int \sigma_{act}\ (E)\ \frac{dE}{E} , \qquad \text{Eq. 26}$$

where

A_∞ = saturation activity, cps.,

N = atoms of In^{115} per $cm.^3$ of foil, and

V = volume of foil, cm.^{3}

The integral in Eq. 26 is the resonance activation cross section integral for In^{115}. This integral was evaluated from the cadmium cut off at 0.4 ev. to infinity. The value of the integral was determined to be 2580 $(10)^{-24}$ cm.^{2} (12, p. 139).

Eq. 26 was then rearranged, so that

$$A_\infty = \frac{m_w W}{(60)(f_t)} = \frac{q}{\xi \Sigma_s} \frac{W}{V} \frac{N_a}{A} \frac{V}{} 2580 (10)^{-24} \qquad \text{Eq. 30}$$

where m_w, W, f_t, N_a, A and V were determined previously to evaluate Eq. 28. When these values were substituted into Eq. 30, $q/\xi \Sigma_s$ was evaluated as follows:

$$\frac{q}{\xi \Sigma_s} = \frac{m_w}{(60)(f_t)} \frac{A}{N_a} \frac{In}{In^{115}} \frac{1}{2580(10)^{-24}} f_e \qquad \text{Eq. 31}$$

$$= \frac{m_w}{(60)(.0454)} \frac{115}{(6.023)(10)^{23}} \frac{1}{.9577}$$

$$\frac{1}{2580 (10)^{-24}} \frac{39}{40}$$

$$= \frac{m_w}{36.1}.$$

The value of $q/\xi \Sigma_s$ was then substituted into Eq. 22 to obtain,

$$\phi_f = (7.26)(2.3) \frac{m_w}{36.1} \qquad \text{Eq. 32}$$

$$= 0.463 (m_w) \text{ fast neutrons/cm.}^2 \text{ sec.}$$

The values of the fast neutron flux, ϕ_f, throughout the moderator are tabulated in Table 3.

Table 3. Fast neutron flux (neutrons/cm.^{2} sec.)

y, in.	0			-6			-12			-18			-24		
x, in.	0	10	20	0	10	20	0	10	20	0	10	20	0	10	20
z, in.															
6	603	322	87	540	290	81	288	172	54	121	85	21	57	33	19
12	368	240	77	332	232	64	191	135	47	102	72	18	53	24	14
18	184	142	49	169	119	45	120	70	36	63	41	14	28	15	12
24	90	61	21	88	51	16	57	45	13	32	30	11	17	10	7
30	26	23	15	23	20	10	22	9	6	20	6	6	16	3	1
36	24	7	2	12	13	0	13	9	3	7	0	3	7	1	0
42	9	7		6	3		6			6			6		
48	8			7											

RESULTS AND DISCUSSION

Thermal Neutron Flux

The experimentally determined values of the thermal neutron flux listed in Table 1 were plotted versus position along each of the three axes to show the distribution of flux throughout the moderator. The distribution of the flux along each of the axes was plotted in Figures 4 through 12.

Figures 4 through 9 showed a trend toward a cosine distribution of thermal flux along the x and y axes. As z increased the distribution approached the theoretical cosine distribution. This was due to the fast neutrons from the source not being slowed down into the thermal region for small values of z. The majority of fast neutrons were thermalized before reaching the z = 18 in. level; essentially all the neutrons were thermalized at the z = 48 in. level.

Figures 10, 11, and 12 showed a trend toward an exponential decrease in flux along the z axis. If the source had been an infinite uniform plane of thermal neutrons, and if the moderator had been infinite, the slope of these curves would have been a straight line. However, the fast neutrons present at low levels of z due to the fast source, and the leakage and deviation of the flux at the finite boundaries caused the flux to be decreased from the theoretical value.

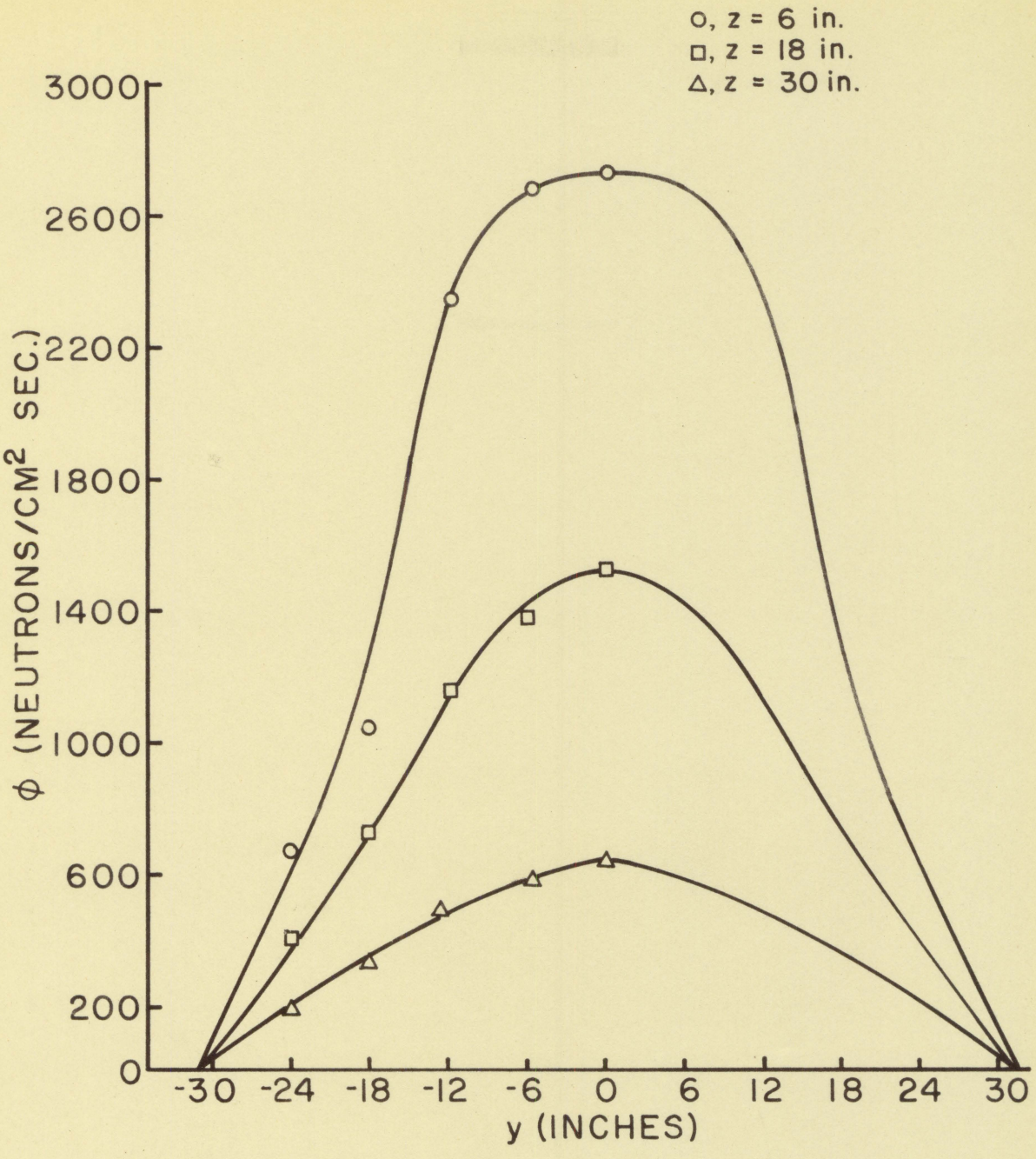

Figure 4. Thermal neutron flux (x = 0 inches)

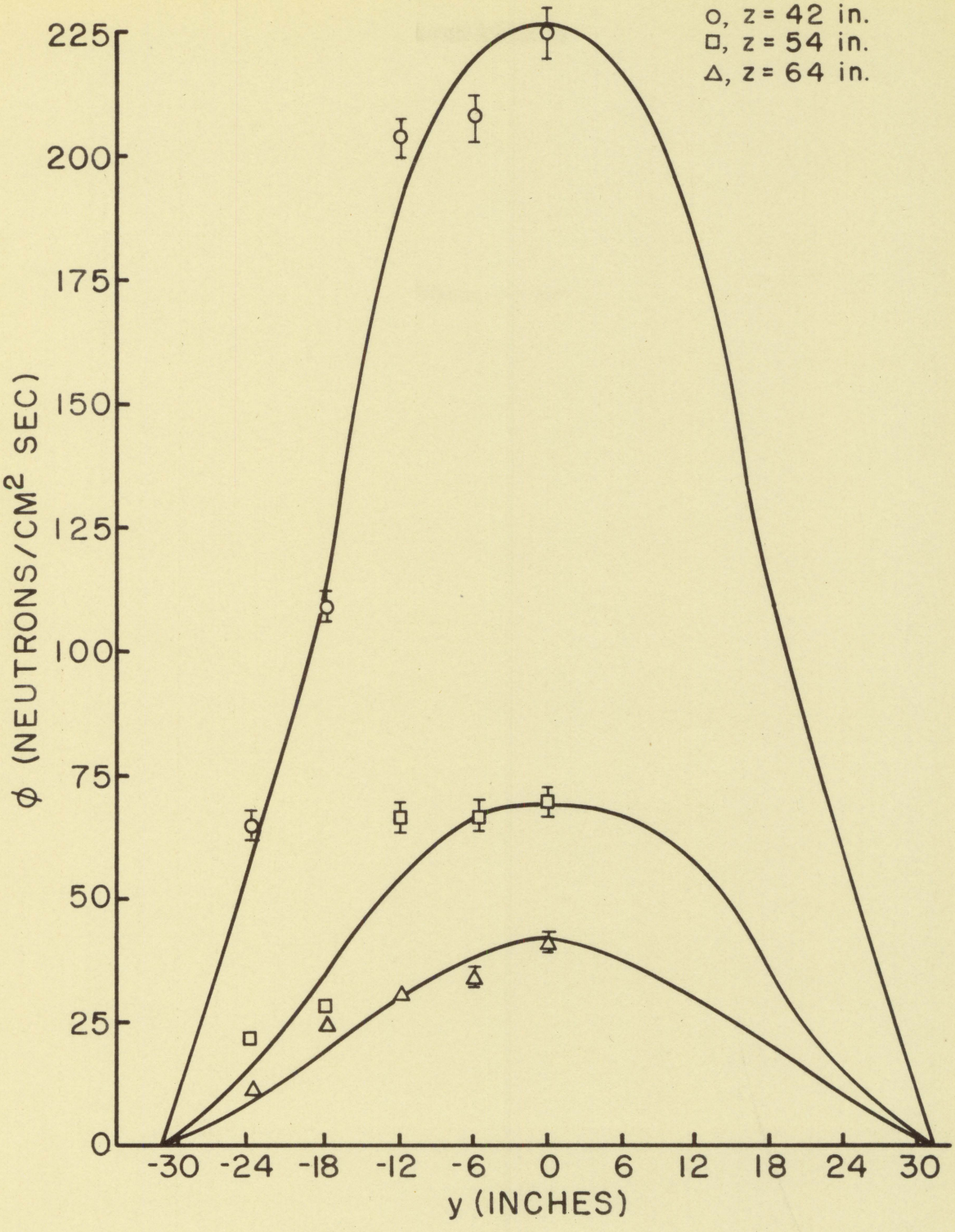

Figure 5. Thermal neutron flux (x = 0 inches)

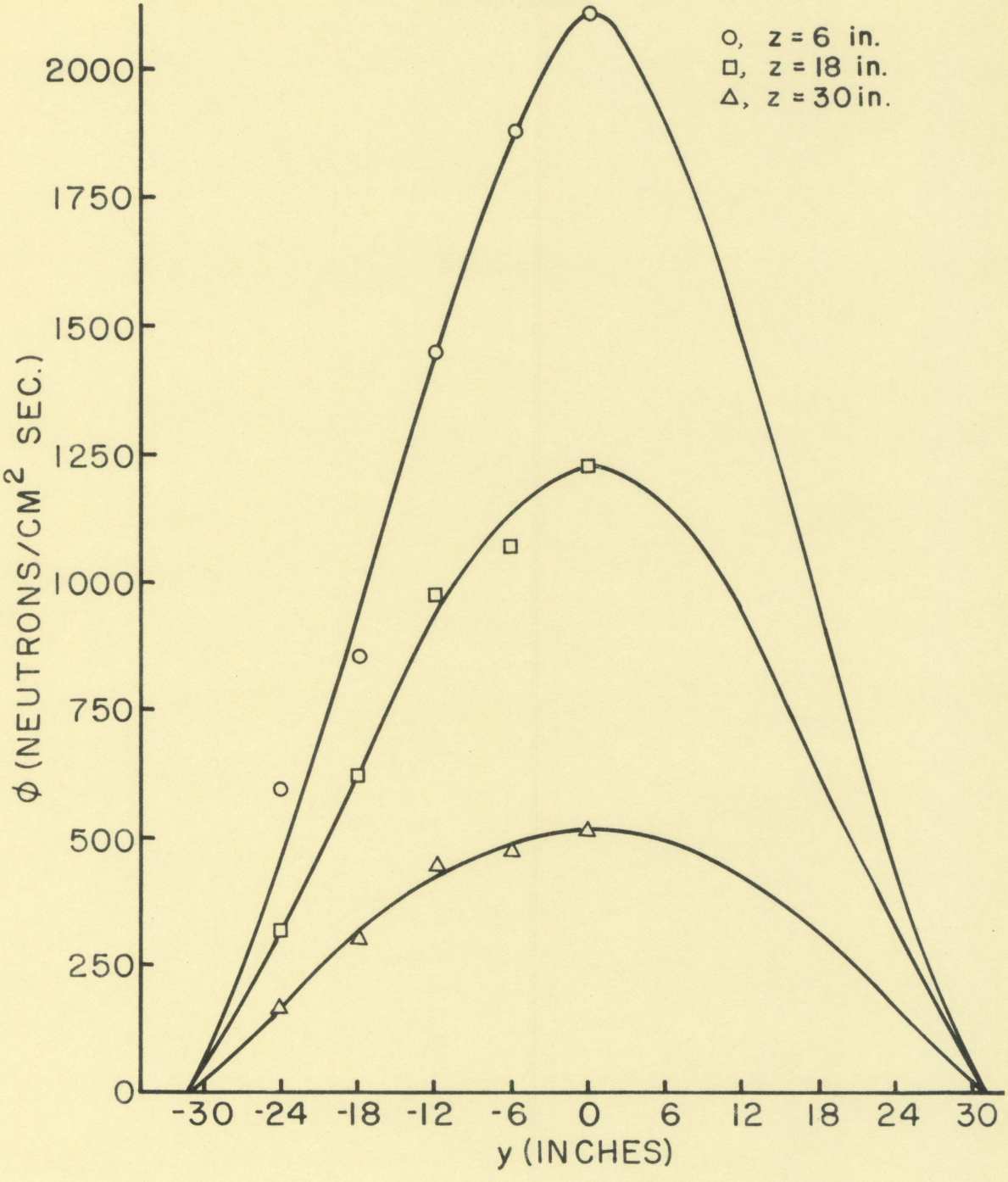

Figure 6. Thermal neutron flux (x = 10 inches)

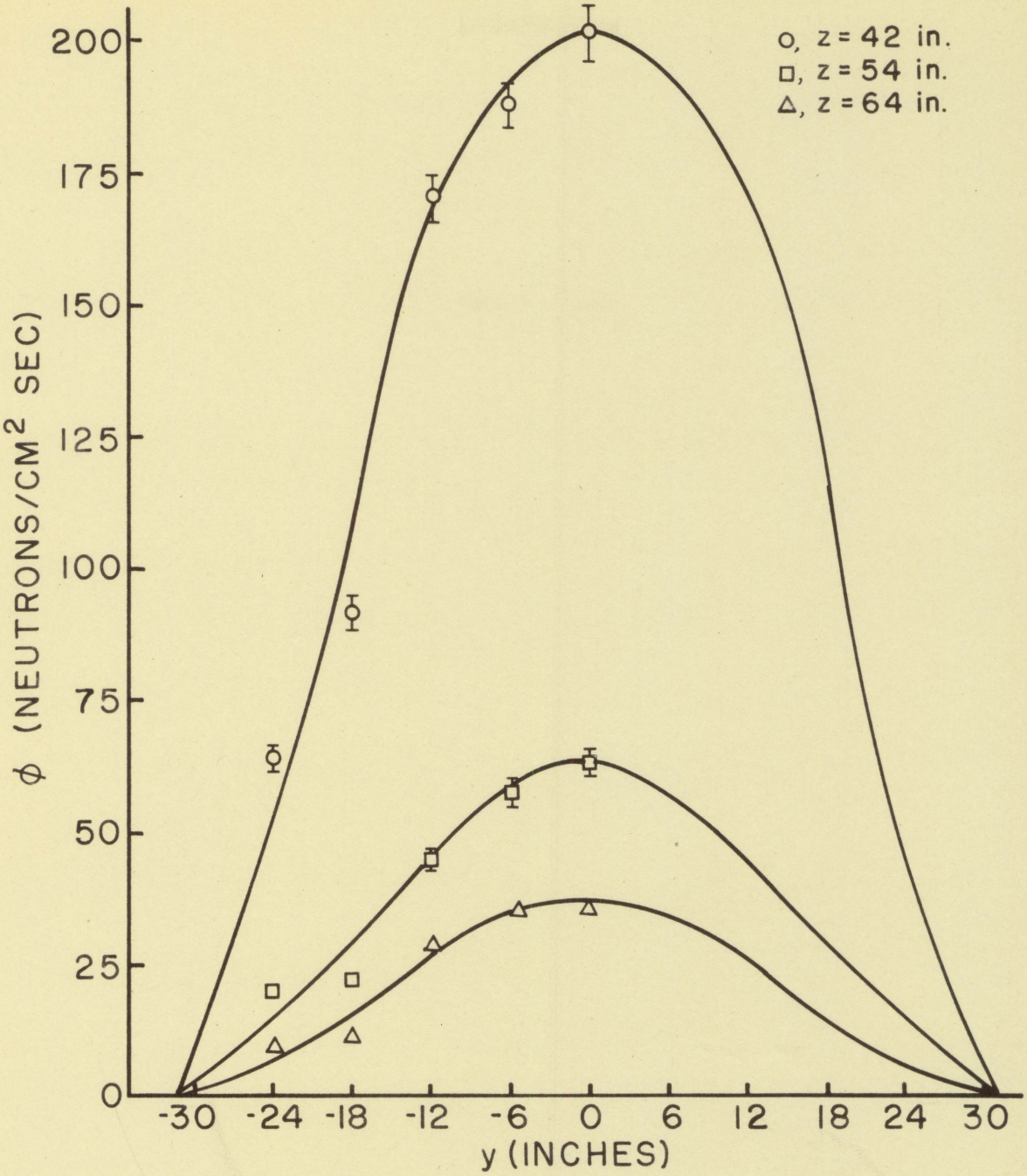

Figure 7. Thermal neutron flux (x = 10 inches)

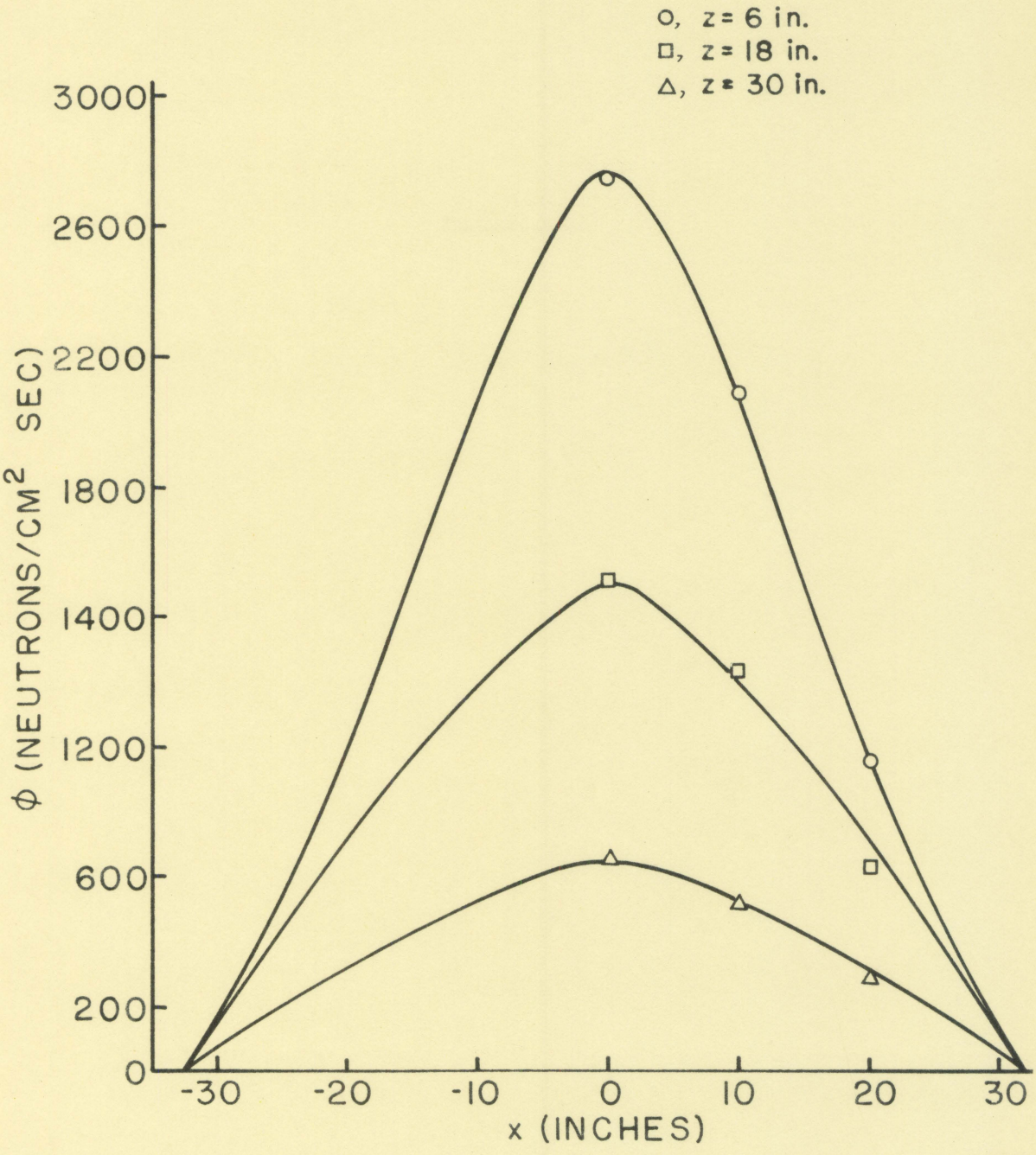

Figure 8. Thermal neutron flux (y = 0 inches)

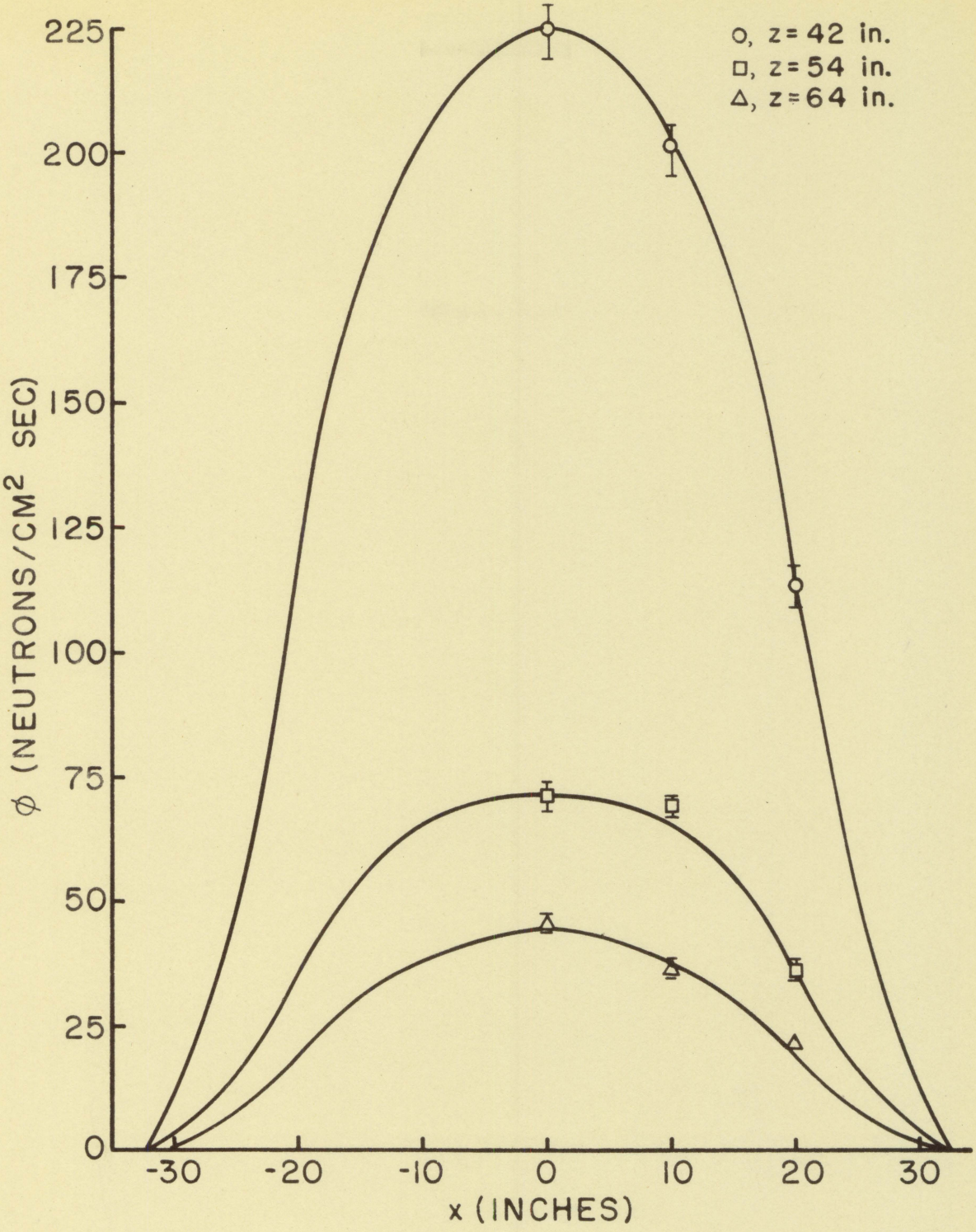

Figure 9. Thermal neutron flux (y = 0 inches)

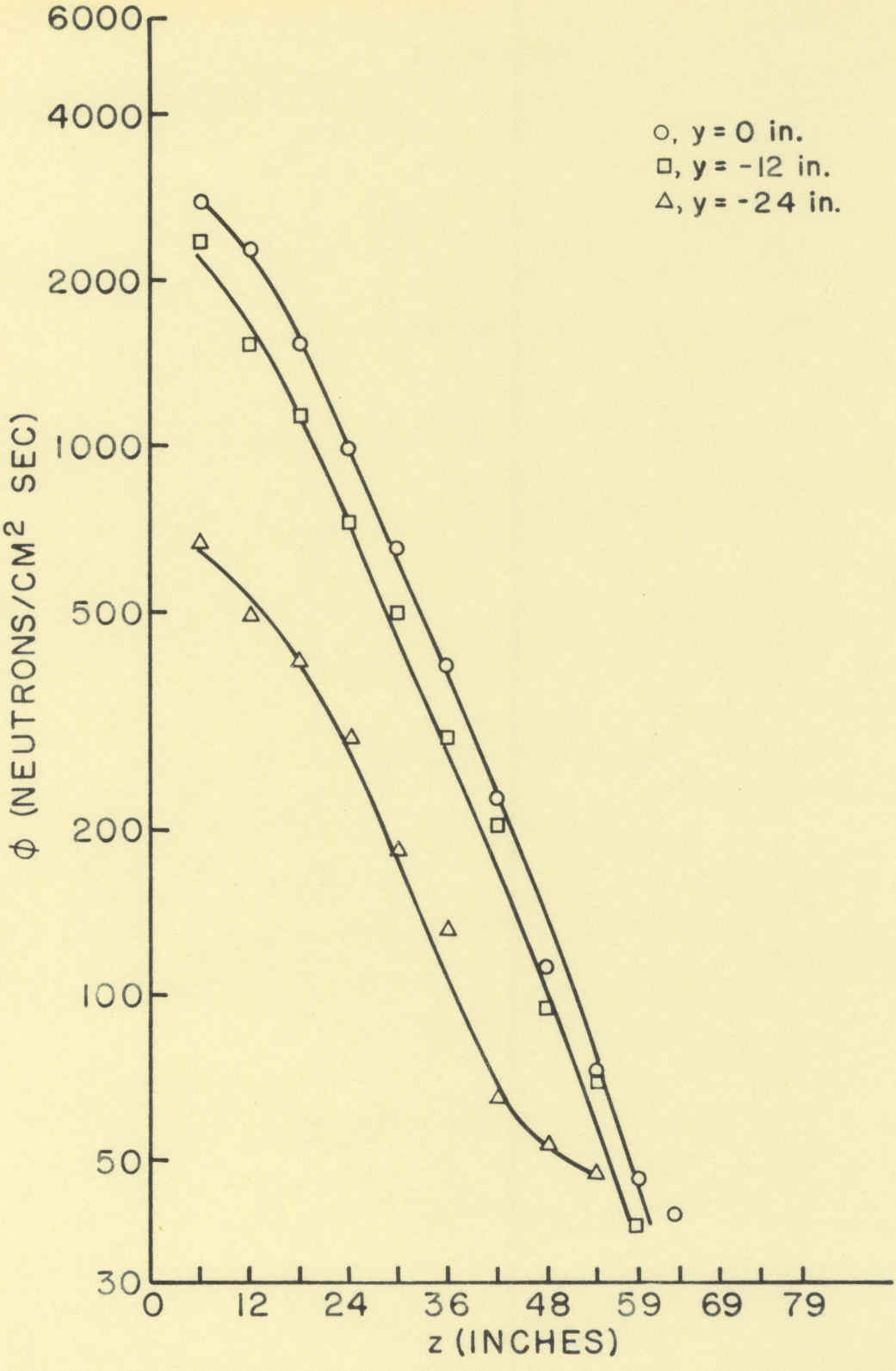

Figure 10. Thermal neutron flux (x = 0 inches)

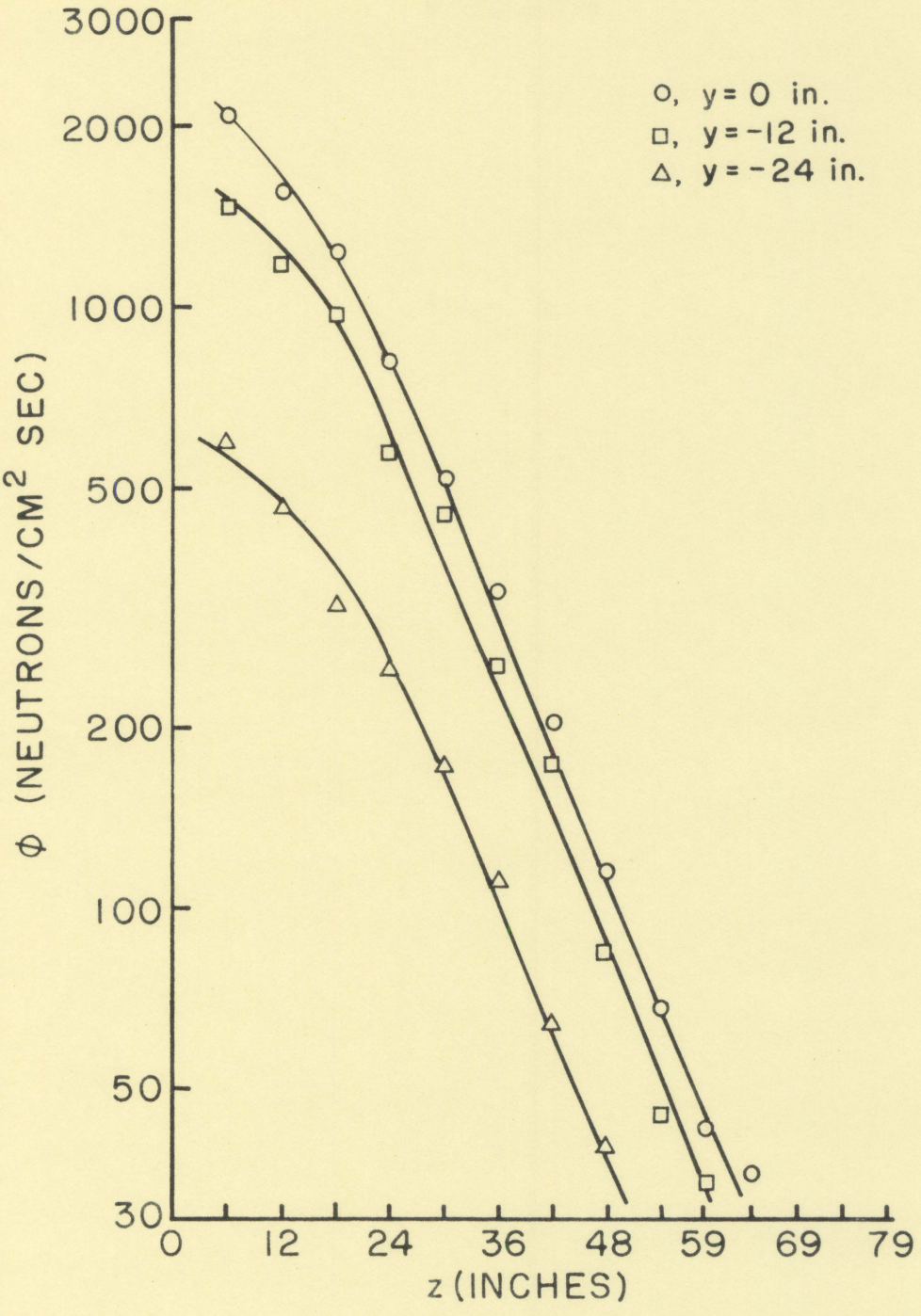

Figure 11. Thermal neutron flux (x = 10 inches)

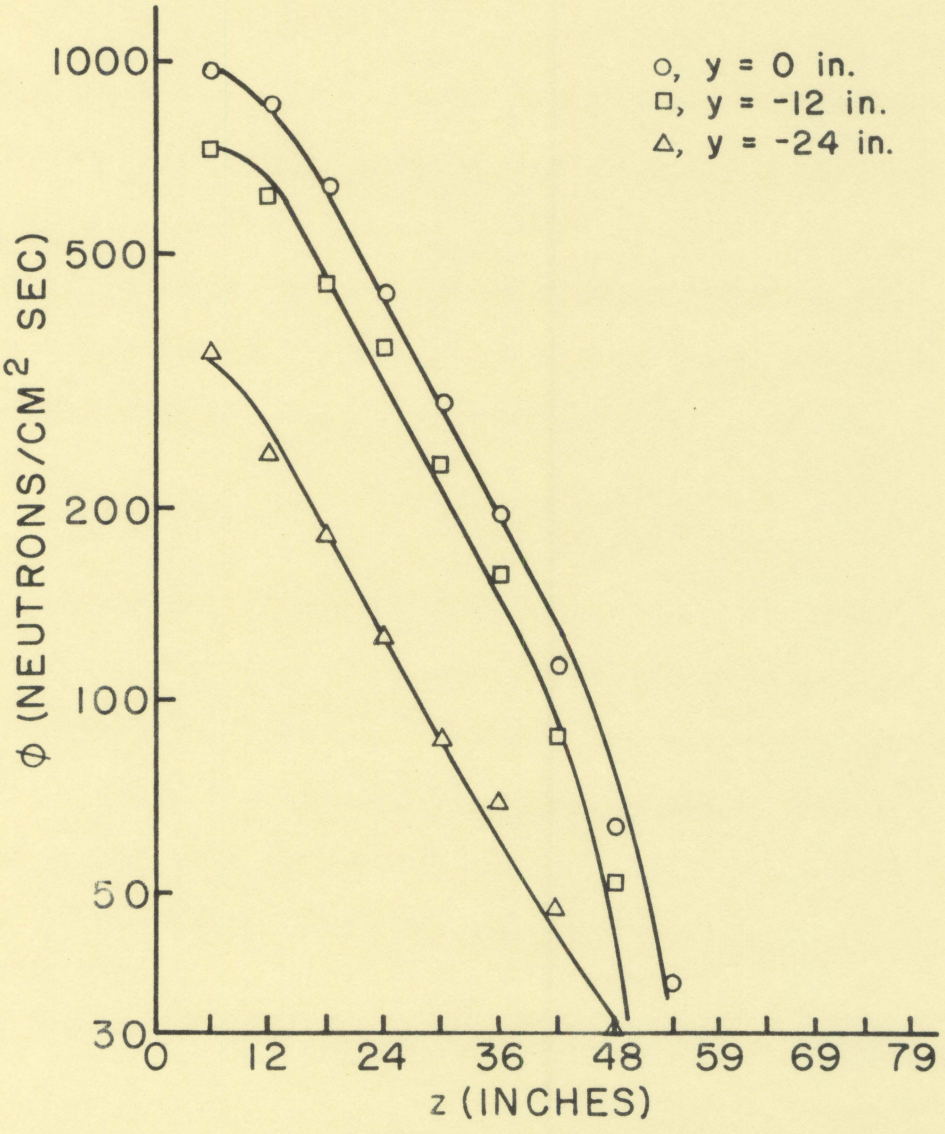

Figure 12. Thermal neutron flux (x = 20 inches)

It was noted that in the center of the moderator, away from all boundaries, the slope was a straight line.

In order to make a direct comparison with the theoretical thermal neutron flux developed in Eq. 14 an equivalent thermal source was calculated from the experimental data. The equivalent thermal neutron source is the constant S in Eq. 14. It represents the number of thermal neutrons emitted per second from a point source at the origin which would give the thermal flux distribution obtained experimentally. From Eq. 14,

$$S = \frac{C\ a\ b\ D\ \gamma_{11}}{2} \quad \frac{\text{thermal neutrons}}{\text{second}}. \qquad \text{Eq. 33}$$

The magnitude of the source depended on the evaluation of the constants in Eq. 33. These constants are related to the geometry, and the material of which the moderator is constructed. The methods used, and the values obtained for these constants are presented in Appendix B. The values of the constants are listed in Table 5, and from Eq. 33,

$$S = 2.992(10)^6 \ \frac{\text{thermal neutrons}}{\text{second}}. \qquad \text{Eq. 34}$$

Eq. 14 was then evaluated to determine the calculated thermal flux distribution of the primary mode.

$$\Phi_{11} = (7593)\ e^{-0.085\ z} \cos \frac{\pi}{64.75} x \cos \frac{\pi}{62.50} y\ . \qquad \text{Eq. 35}$$

The values of Φ_{11} were calculated for various values of x, y, and z to show the distribution of thermal flux. The results

of these calculations are tabulated in Table 4.

The experimental thermal neutron flux values listed in Table 1 are $\sum_{m=1}^{\infty}\sum_{n=1}^{\infty}\phi_{mn}$ which included the effects of harmonics and end corrections. The harmonic and end correction factors were calculated and tabulated in Table 4. The $\sum_{m=1}^{\infty}\sum_{n=1}^{\infty}\phi_{mn}$ flux was divided by the corresponding harmonic and end correction factors to obtain experimental values of ϕ_{11} to compare with the calculated values. The results of these calculations are listed in Table 4. The calculated and experimental values of ϕ_{11} were compared in Figures 13, 14 and 15. Figures 13 and 14 showed the distribution of flux along the x axis with y = 0, and z = 36 in., and along the y axis with x = 0 and z = 26 in. Figure 15 compared the distribution of flux along the z axis with x = y = 0. The experimentally determined flux compared favorably with the calculated flux along the x and y axes. In the center of the moderator the comparison was good along the z axes. However, near the source the comparison was poor. This was due to the effects of the fast neutron source. By the time the fast neutrons had reached z = 18 in., the majority of them were slowed down to thermal energies. The deviation of experimental flux from the calculated, at large values of z, was due primarily to the statistics of counting. The activity at values of z greater than 59 inches was so small that it was not possible to obtain an accurate measurement.

Table 4. Harmonic and end corrections and Φ(neutrons/cm.^{2} sec.)

		Ch	Ce	(Ch)(Ce)	Φ_{mn} experimental	Φ_{11} experimental	Φ_{11} calculated
x = 0 in.	z, in.						
y = 0 in.	6	1.8295	1.0000	1.8295	2750	1505.0	4550
	12	1.5125	1.0000	1.5125	2240	1481.0	2738
	18	1.2908	1.0000	1.2908	1521	1181.0	1645
	24	1.1579	0.9999	1.1577	994	859.9	986
	30	1.0939	0.9996	1.0930	648	594.5	585
	36	1.0571	0.9991	1.0580	390	368.2	359
	42	1.0349	0.9976	1.0320	225	217.9	214
	48	1.0210	0.9937	1.0150	121	119.2	128
	54	1.0130	0.9836	0.9965	70	70.3	77.3
	59	1.0080	0.9705	0.9705	47	48.3	50.8
	64	1.0010	0.9310	0.9311	41	44.1	33.4
	69	1.0000	0.8390	0.8390	29	34.6	21.6
	74	1.0000	0.6235	0.6235	19	30.5	14.2
x = 0 in.	y, in.						
z = 36 in.	0	1.0571	0.9991	1.0560	390	368.2	359.0
	-6	1.0519	0.9991	1.0511	373	354.2	342.0
	-12	1.0202	0.9991	1.0193	297	292.0	295.6
	-18	0.9806	0.9991	0.9798	256	261.8	222.0
	-24	0.9472	0.9991	0.9465	131	138.4	128.5
y = 0 in.	x, in.						
z = 36 in.	0	1.0571	0.9991	1.0560	390	368.2	359.0
	+10	1.0347	0.9991	1.0342	335	324.0	318.5
	+20	0.9723	0.9991	0.9718	194	199.5	203.0

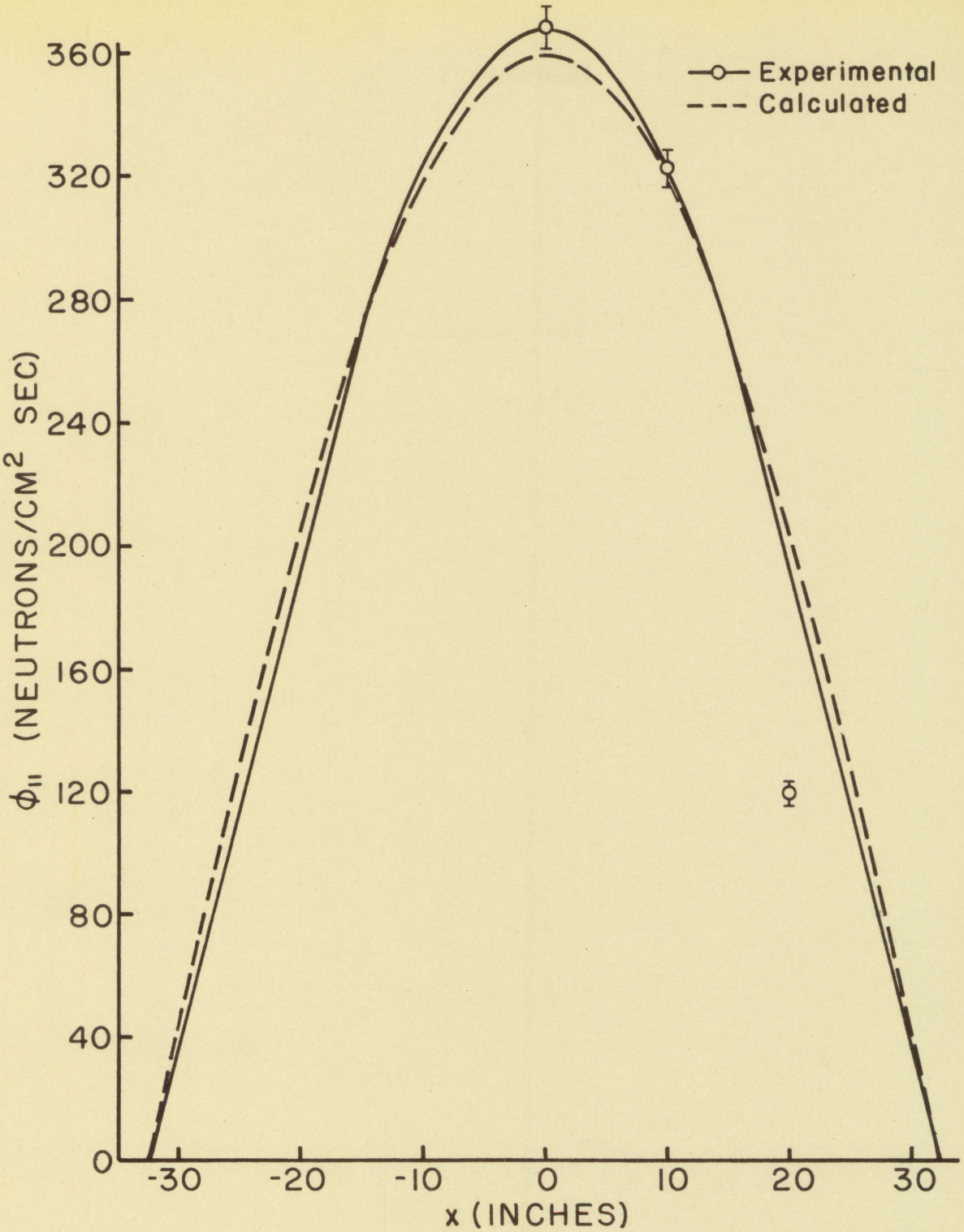

Figure 13. Calculated and experimental thermal neutron flux (y = 0, z = 36 inches)

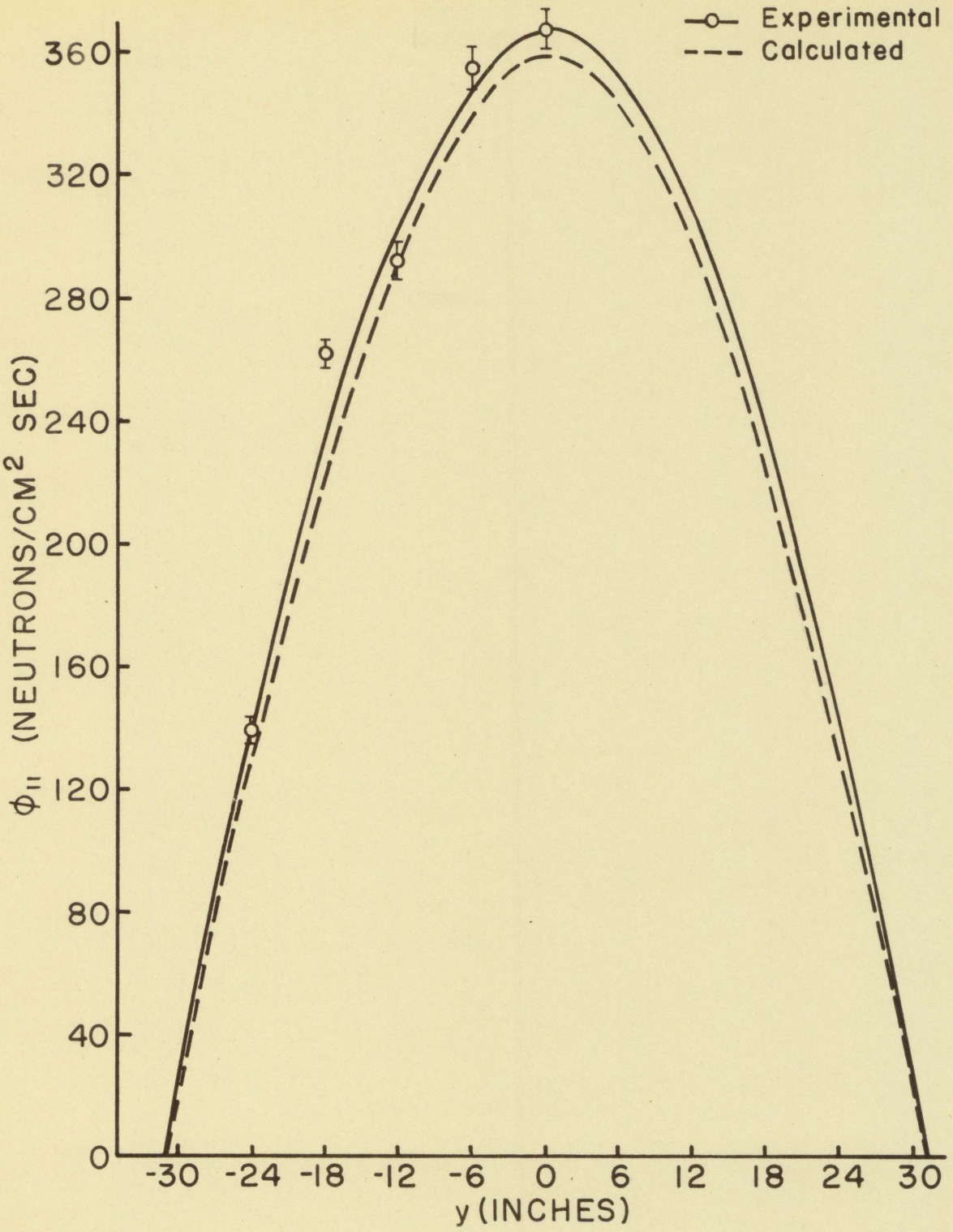

Figure 14. Calculated and experimental thermal neutron flux (x = 0, z = 36 inches)

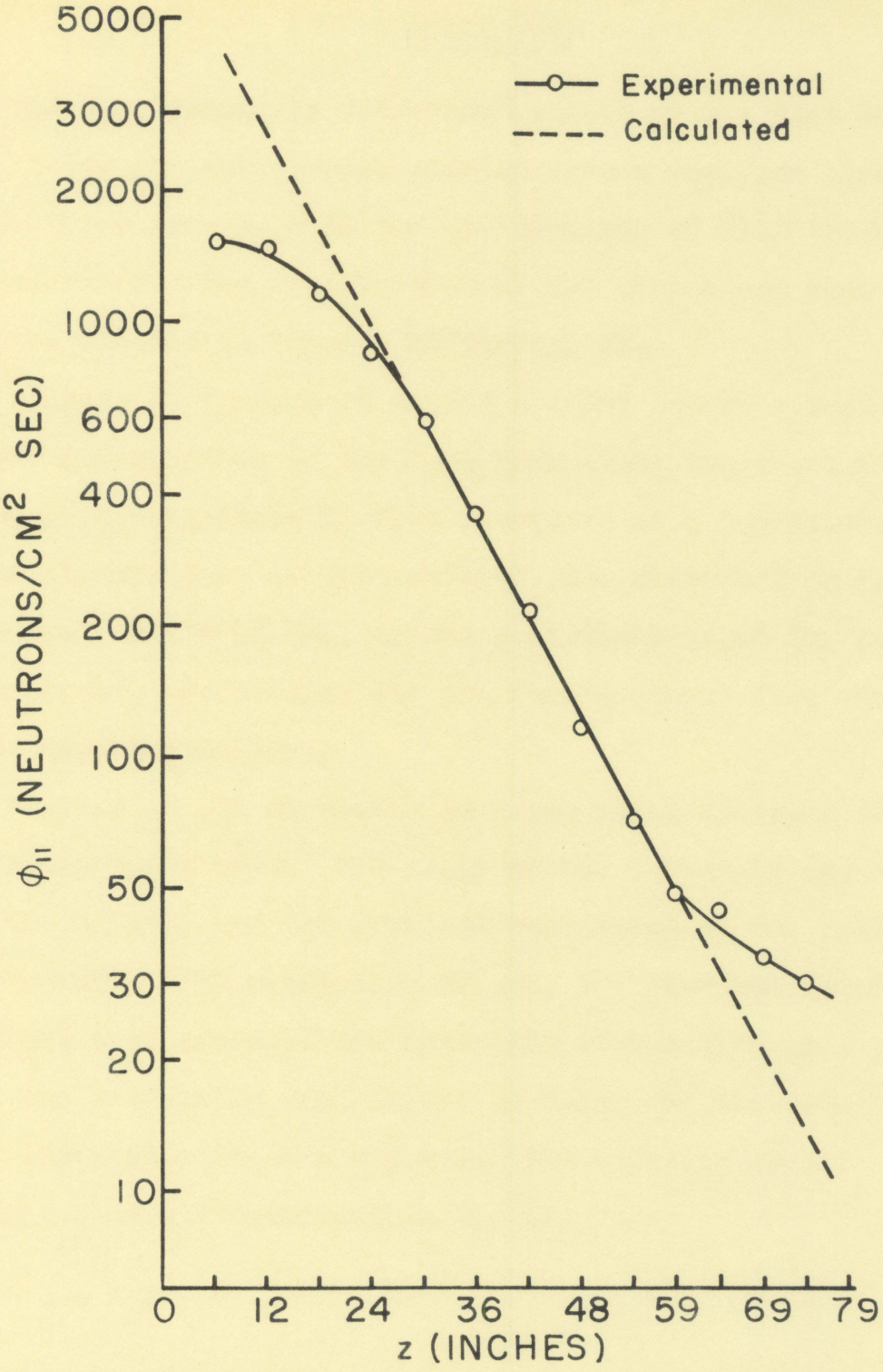

Figure 15. Calculated and experimental thermal neutron flux (x = 0, y = 0 inches)

Fast Neutron Flux

The experimentally determined values of the fast neutron flux listed in Table 3 were plotted versus position along each of the three axes to show the distribution of flux throughout the moderator. The distribution of the flux along each of the axes was plotted in Figures 16 through 21.

Figures 16 through 19 showed a trend toward a cosine squared distribution of the fast flux along the x and y axes. Although the magnitude of flux decreased as z increased, due to the slowing down of the neutrons, the distribution remained the same. At z = 48 in., or the equivalent of 48 in. from the point source, essentially all the fast neutrons from the source were thermalized.

Figures 20 and 21 showed an exponential decrease in the flux along the z axis. The slope of the curves 18 in. away from the source, and the physical boundaries of the moderator was constant. The relaxation length, the distance required in graphite to decrease the intensity of the flux by a factor of e, was calculated from Figure 20 using the distribution along the z axis where x = y = 0. The equation of the straight line was developed in Eq. 12.

$$\Phi_f = C\, e^{-\gamma z} \qquad \text{Eq. 36}$$

$$140 = C\, e^{-\gamma (20)} \qquad \text{Eq. 37}$$

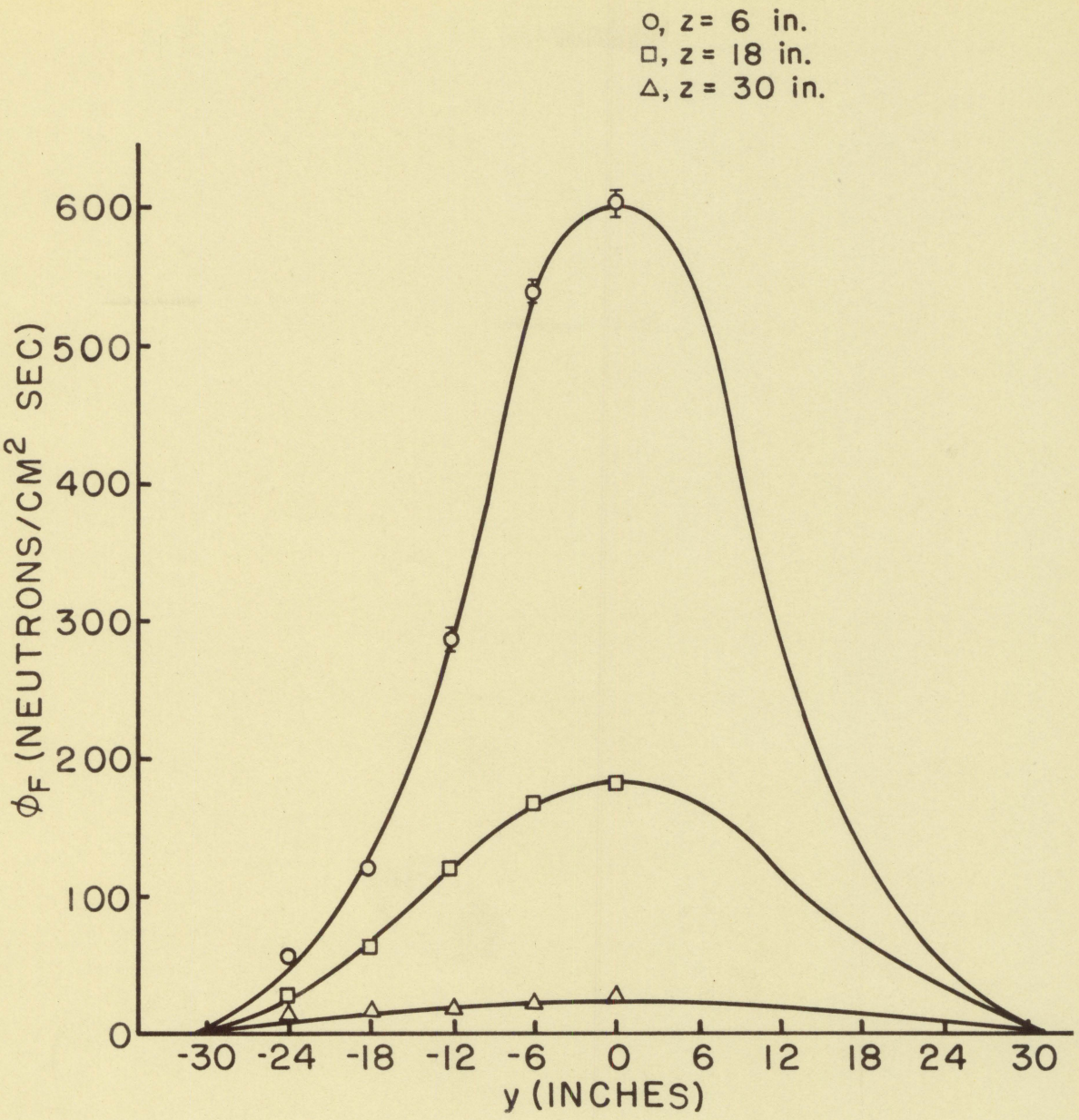

Figure 16. Fast neutron flux (x = 0 inches)

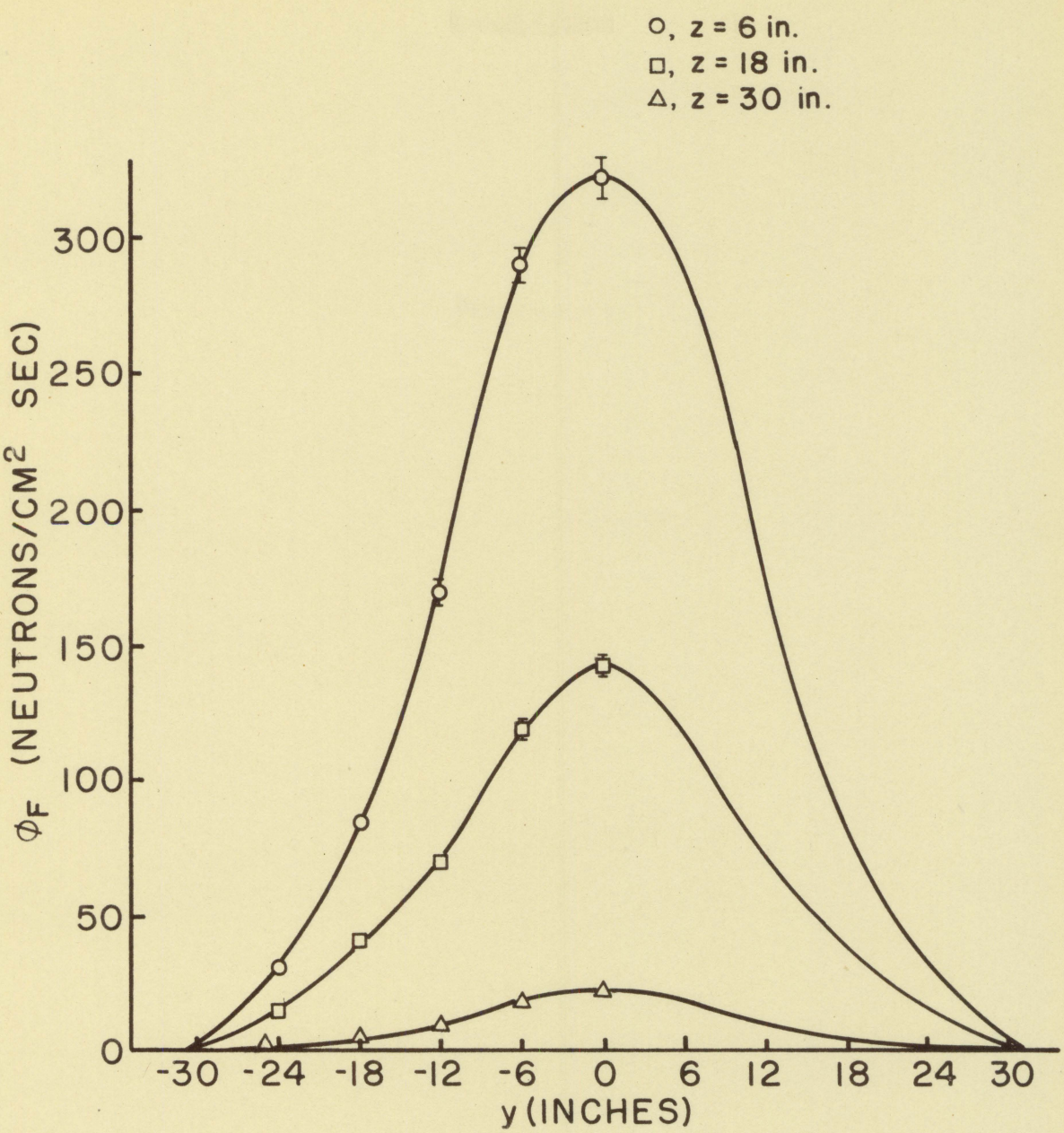

Figure 17. Fast neutron flux (x = 10 inches)

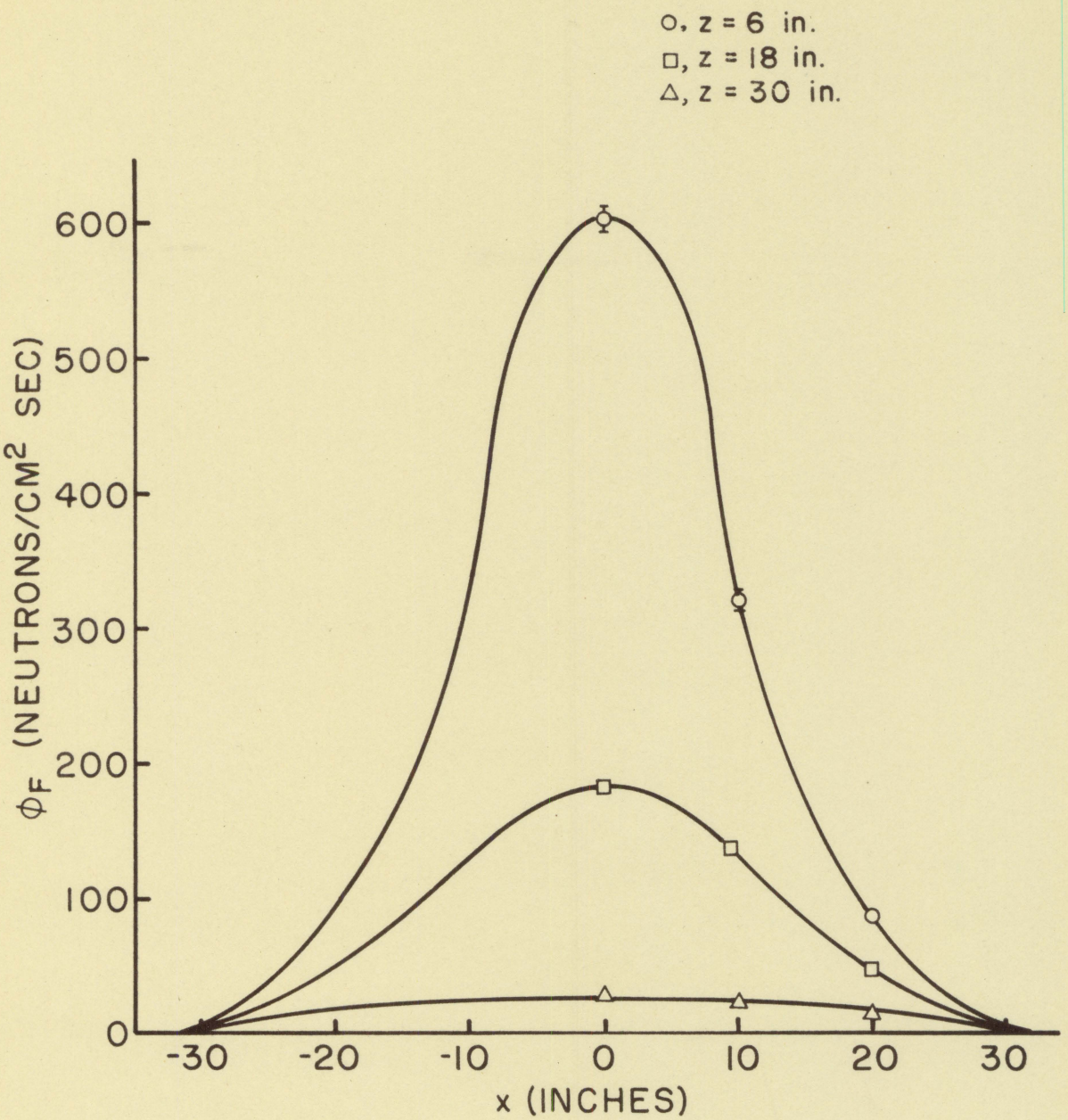

Figure 18. Fast neutron flux (y = 0 inches)

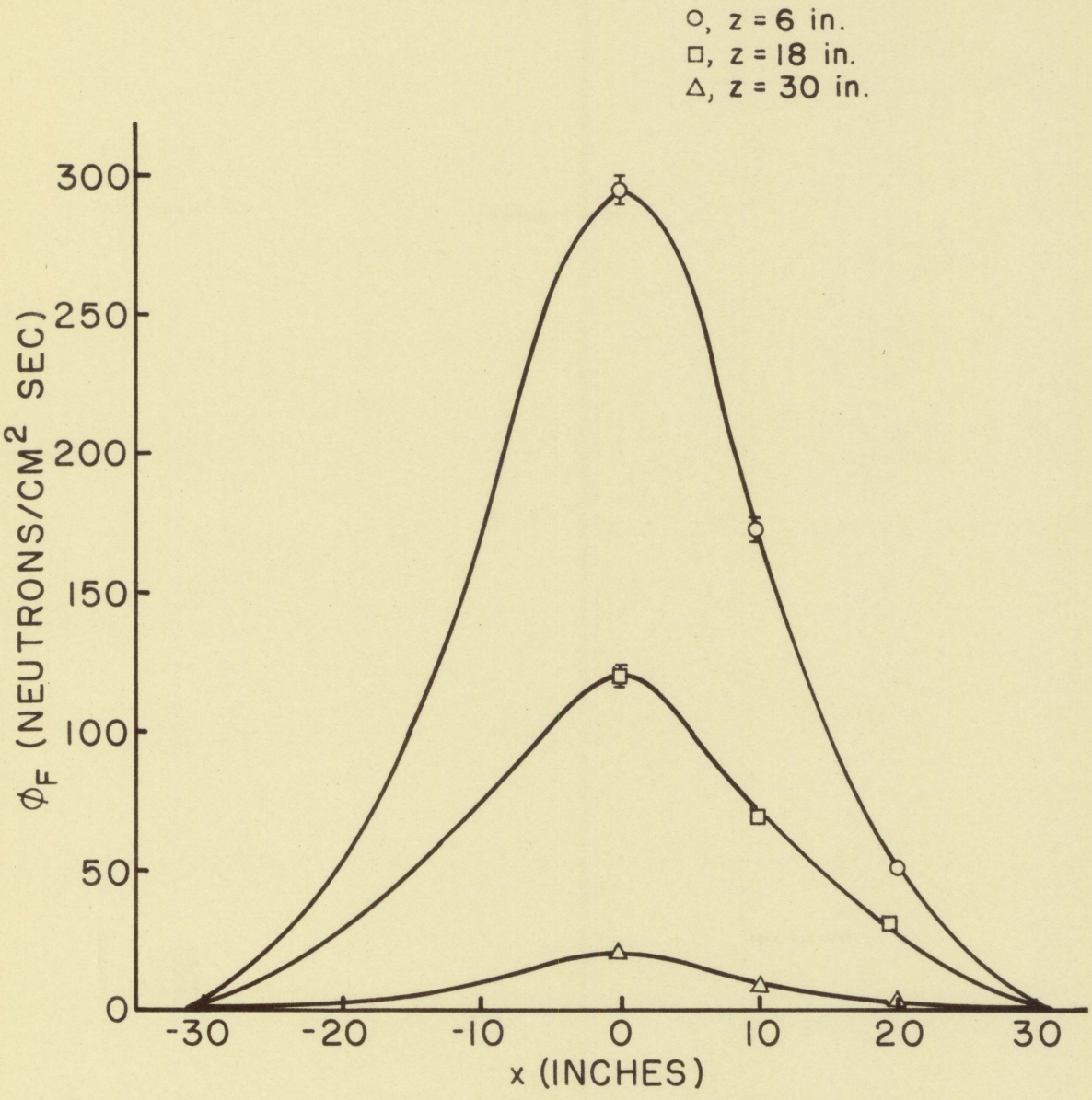

Figure 19. Fast neutron flux (y = -12 inches)

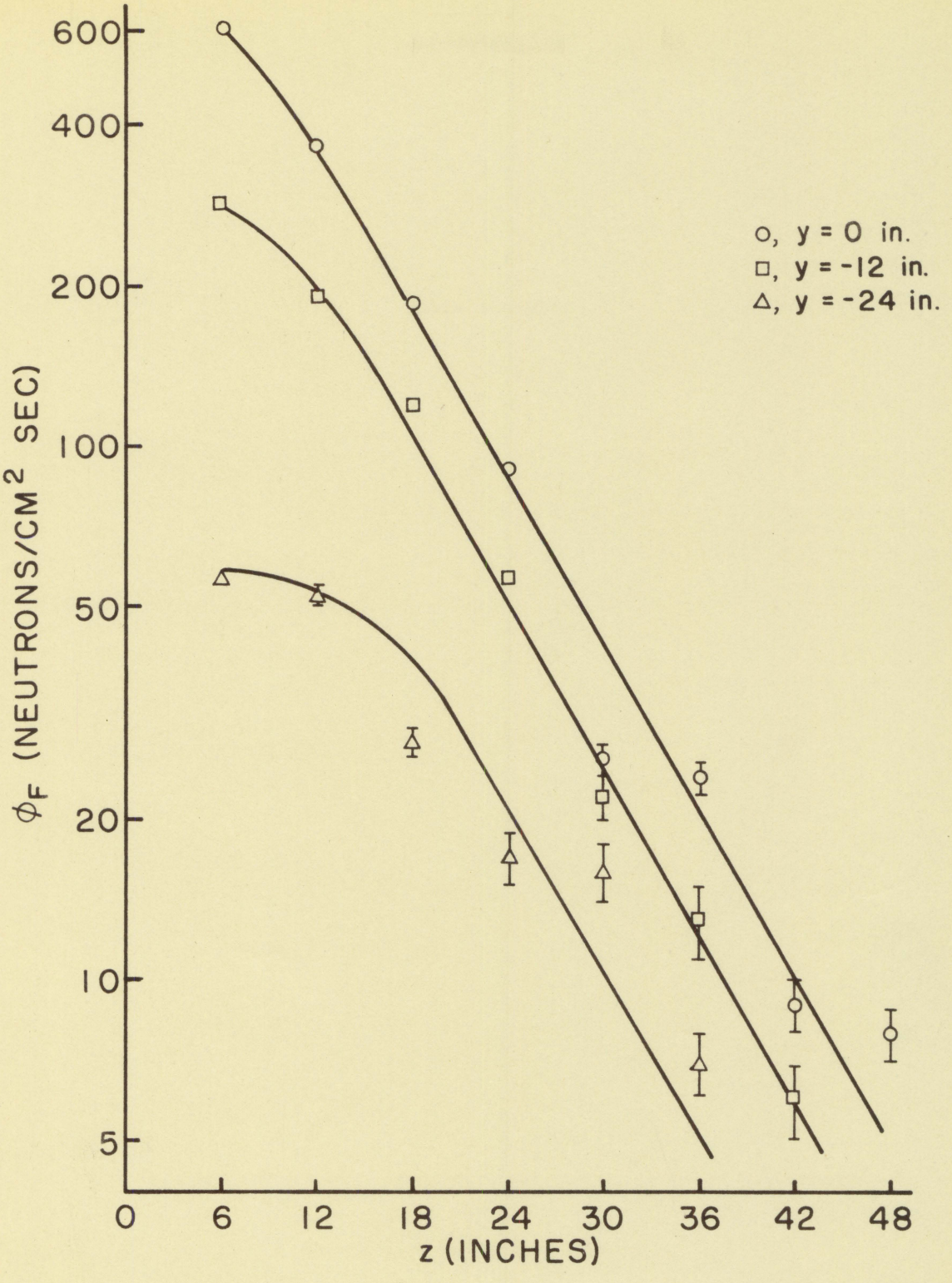

Figure 20. Fast neutron flux (x = 0 inches)

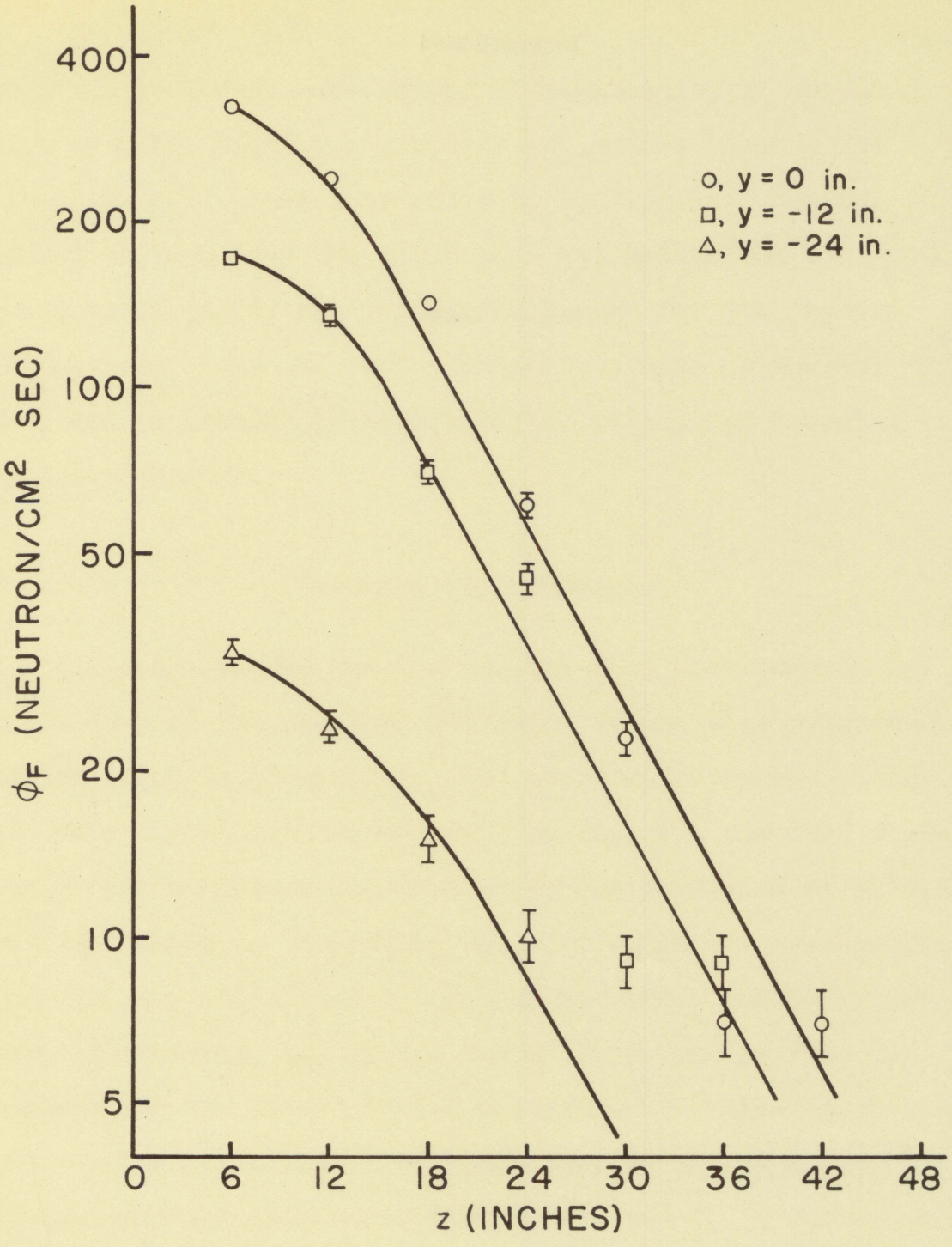

Figure 21. Fast neutron flux (x = 10 inches)

$$10 = C\, e^{-\gamma(42)} \qquad \text{Eq. 38}$$

Equations 37 and 38 were solved simultaneously to obtain a value of 0.120 in.$^{-1}$ for γ. The relaxation length, the reciprocal of γ, was determined to be 8.33 in. For the thermal neutron flux the value of γ_{11}, determined in Appendix B, was 0.085 in.$^{-1}$; the relaxation length for the thermal neutrons was 11.76 in. The relaxation length of thermal neutrons was 41 percent greater than the relaxation length of the fast neutrons.

Accuracy of Results

The methods used and the results obtained from the determination of the standard deviation in the flux measurements are presented in Appendix C. The standard deviation of the flux values were determined from Eq. 51. The standard deviation of the component was divided by the component to obtain the coefficient of variation, C_v. The C_v in the calibration procedure was calculated to be 11.1 percent. The C_v of the measured activity, m_w, of the indium foils varied from 0.1 percent near the source to 8.2 percent near the boundaries of the moderator. The C_v in the calibration procedure was constant for all flux measurements, but the C_v in the measured activity increased with distance from the source. Therefore, the C_v in flux measurements varied from 11.2 percent close to

the source to 19.3 percent near the boundaries of the moderator. In the vicinity of the center of the moderator the C_v was 12.9 percent.

The vertical bars superimposed upon the experimental points which have been presented graphically in this thesis represent the standard deviation of the measured activity. Where bars have not been shown, the deviation is less than the size of the symbol.

CONCLUSIONS

Thermal and fast neutron fluxes in a graphite moderator with a fast, external, neutron source can be measured by utilizing a combination of activated indium foils and a calibrated counter.

The thermal flux distribution in this graphite moderator agreed very well with the theory. A cosine distribution about the x and y axes and an exponential variation along the z axis was obtained. This was strictly true only for flux measurements taken more than 18 inches from the source, and away from the physical boundaries of the moderator. The strength of the equivalent thermal source was $2.992(10)^6$ neutrons per second. The relaxation length in graphite was 11.76 inches.

The fast neutron flux varied in an approximate cosine squared distribution about the x and y axes, and exponentially along the z axis. Within 18 inches of the source the variation along the z axis was not exponential. Essentially all fast neutrons were thermalized after passing through 48 inches of the moderating material. The relaxation length of the fast neutrons in graphite was 8.33 inches.

The coefficient of variation in the determination of the neutron fluxes varied from 11.2 percent close to the source

to 19.3 percent near the boundaries of the moderator. In the center of the moderator the C_v was 12.9 percent.

SUGGESTIONS FOR FURTHER STUDY

Further investigation into the fast neutron flux distribution could be carried out by obtaining the energy spectrum of the neutrons throughout the moderator. The energy spectrum of the source is known, and the change in the spectrum due to the slowing down of neutrons could be obtained by activation techniques. This could be accomplished by taking a series of measurements with a variety of foils with different resonance peaks. The energy spectrum might also be obtained with a spectrometer.

If the variation of the energy spectrum throughout the moderator were known, a more accurate fast neutron flux distribution could be obtained. Since the microscopic cross section varies with the energy of the neutron, the energy spectrum would provide the means of obtaining an accurate value of the cross section.

LITERATURE CITED

1. Baughman, F. H. Operating characteristics of a uranium graphite subcritical assembly. Unpublished M. S. Thesis. Ames, Iowa, Iowa State College Library. 1957.

2. Bleuler, E., and Goldsmith, G. J. Experimental nucleonics, New York, N. Y., Rinehart and Co., Inc. 1952.

3. Dana, F. C., and Hillyard, L. R. Engineering problems manual. New York, N. Y., McGraw-Hill Book Co., Inc. 1947.

4. Davenport, D. E., Lynn, G. L., and Pound, D. C. Hanford standard pile. U. S. Atomic Energy Commission. Report HW-21793 [Hanford Works, Richland, Washington].

5. _____, _____, and Richey, C. R. The standardization (nv/q) of gold and indium foils and the absolute neutron flux determination in the Hanford standard pile. U. S. Atomic Energy Commission. Report HW-26207 [Hanford Works, Richland, Washington]. 1954.

6. Davis, M. V., and Hauser, D. T. Thermal-neutron data for the elements. Nucleonics. 16: 87-90. 1958.

7. Friedlander, G., and Kennedy, J. W. Nuclear and radiochemistry. New York, N. Y., John Wiley and Sons, Inc. 1955.

8. Glasstone, S., and Edlund, M. C. The elements of nuclear reactor theory. Princeton, N. J., D. Van Nostrand Co., Inc. 1952.

9. Greenfield, M. A., Koontz, R. L., and Jarrett, A. A. Absolute thermal neutron determination. Part I: Measuring the ratio of thermal to resonance neutron densities using thick indium foils. U. S. Atomic Energy Commission Report NAA-SR-1137. [North American Aviation, Inc., Downey, California]. 1955.

10. _____, _____, and _____. Absolute thermal neutron determination. Part III: Absolute thermal neutron flux. [U. S. Atomic Energy Commission Report]

NAA-SR-1137. [North American Aviation, Inc., Downey, California]. 1957.

11. Hoag, J. B. Nuclear reactor experiments. Princeton, N. J., D. Van Nostrand Co., Inc. 1952.

12. Hughes, D. J. Pile neutron research. Cambridge, Mass., Addison-Wesley Co., Inc. 1953.

13. _____, and Schwartz, R. B. Neutron cross sections. 2nd ed. Washington, D. C. U. S. Govt. Print. Off. 1958.

14. Klema, E. D., Ritchie, R. H., and McCammon, C. Recalibration of the X-10 standard graphite pile. [U. S. Atomic Energy Commission Report] ORNL-1398. Oak Ridge National Laboratory. 1952.

15. Koontz, R. J., Greenfield, M. A., and Jarrett, A. A. Absolute thermal neutron determination. Part II: Absolute beta counting of indium foils. [U. S. Atomic Energy Commission Report] NAA-SR-1137. [North American Aviation, Inc., Downey, California]. 1955.

16. Stewart, Leona. Neutron spectrum and absolute yield of a plutonium-beryllium source. Physical Review. 98: 740-743. 1955.

17. Worthing, A. G., and Geoffner, J. Treatment of experimental data. New York, N. Y., John Wiley and Sons, Inc. 1943.

ACKNOWLEDGEMENTS

The author wishes to acknowledge with grateful thanks the assistance received from the various members of the staff affiliated with Nuclear Engineering. In particular I would like to express my deep gratitude to Dr. Robert E. Uhrig for the original suggestion of this project, and his continued active interest directed toward its accomplishment. To Dr. Glenn Murphy are due my thanks for help and encouragement throughout my stay at Iowa State College. I wish to thank Dr. Adolf Voigt for the assistance received in preparing a standard source.

This thesis represents the conclusion of three years of postgraduate education sponsored by the United States Navy. I wish to express my appreciation to the United States Naval Postgraduate School as well as the United States Navy for the two years work in Aeronautical Engineering at Monterey, California, and for the third year in Nuclear Engineering at Iowa State College.

APPENDIX A: CALIBRATION OF COUNTER

Preparation of Standard

To determine the neutron flux it was necessary to obtain a comparison between the actual disintegration rate, and the measured activity of the indium. This was accomplished by calibrating the counter with a standard sample.

The liquid thallium used as a standard was prepared by Bureau of Standards, Washington, D. C. in April 1953. Thallium was utilized as a standard because its β activity is similar to that of indium. The average energy of the indium β is 0.9 Mev.; the average energy of the thallium β is 0.764 Mev. Thallium contains no other contaminating radiation particles. The β has a half life of 4.0 years, so it was considered an ideal standard.

An aluminum planchet 1.75 in. by 1.25 in. by 0.02 in. was used to mount the standard. The same size planchet was used for mounting the indium foils, so background and back scattering effects were the same for the indium and thallium. The planchet was cleaned with carbon tetrachloride. A strip of scotch tape, the same area as the indium foil, was placed on the planchet; the planchet was then sprayed with kyrlon. The kyrlon formed a border around the planchet leaving the desired interior area for the thallium standard after removal

of the tape.

The original thallium sample had a β activity of 11,430 disintegrations per second per milliliter as of April, 1953. An approximate determination of counter efficiency and sample strength showed that 100 microliters of the thallium would produce an activity comparable to the activated indium foils. A 100 microliter sample was pipeted from the source and deposited on the prepared aluminum planchet. Two distilled water rinsings were also deposited on the planchet to ensure that all the radioactivity removed from the thallium source was actually received by the planchet. Two drops of Aerosol, a spreading agent, were then added to the solution. The solution was distributed evenly within the borders of the planchet with a glass stirring rod. The rod was rinsed with distilled water, and the rinsings were added to the solution. The solution was placed under a heat light; the water was evaporated, and a uniform thin layer of thallium remained on the planchet.

Activity of Standard Sample

The activity of the 100 microliter prepared sample was 1143 disintegrations per second at the time of its original preparation, April, 1953. This standard sample can be used for future calibrations by calculating its current activity

due to the β decay with a half life of 4.0 years. The disintegration rate of the standard sample was calculated to be 25,740 counts per minute as of 8 December, 1958.

The activity of the standard thallium sample was then measured with the same counter configuration and geometry used for determining the activity of the indium foils. The aluminum planchet was inserted in the holder, and a series of long counts were taken; the average was 1753 cpm. The planchet was turned 180 degrees, and a second series of counts averaged to 1845 cpm. The average count rate for the two possible geometric arrangements was 1799 cpm. which was utilized to calibrate the counter. The 2.55 percent deviation from the average count rate for each configuration was an indication of the uniformity of density of the activity on the prepared standard. The average activity was then corrected for dead time and background, and the net measured activity was determined to be 1774 cpm.

Evaluation of Correction Factors

The various counting correction factors were determined for the standard. Corresponding factors were then applied to the measured saturated activity of the indium foils to determine the actual saturation activity. These correction factors were determined in accordance with the experimental procedures

set forth by Bleuler and Goldsmith (2).

The relationship of the factors follow (2, p. 95):

$$m = (A_\infty)(f_e)(f_\tau)(f_g)(f_w)(f_b)(f_s) \qquad \text{Eq. 39}$$

where

m is the net measured activity, cpm.,

A_∞ is the actual saturation activity, cpm.,

f_e is the efficiency factor, ratio of observed counts, to the actual number of particles which enter the counting volume,

f_τ is the dead time correction factor, dead time corrections were applied before arriving at a net counting rate, so it can be considered as unity,

f_g is the true geometry factor, fraction of total solid angle which is subtended by the active area of the counter,

f_w is the absorption factor, ratio of activity arriving at counter to that emitted,

f_b is the back scattering factor, ratio of activity counted on the standard mounting to that on a weightless mounting, and

f_s is the self absorption factor, fraction of activity absorbed by the radioactive material being counted.

Since the geometry, f_g, the backing and mounting of the sample, f_b, and the efficiency of the counter, f_e, were

identical for the thallium sample and the indium foils, they were combined as one correction factor. Thus, $(f_g)\cdot(f_b)\cdot(f_e)$ equaled f_1; f_1 was calculated for the thallium standard and the same correction was applied to the indium foils.

The thallium sample was very thin and essentially weightless, so f_s was assumed to be unity. The factor f_w for thallium was determined from an absorption curve. This was accomplished by measuring the activity which passed through a range of added aluminum absorbers. These activities were plotted on a semi log plot versus added absorber thickness on Figure 22. The best straight line was drawn through the points; this line was extended to zero added absorber, and then to zero total absorber. The difference between zero added and zero total absorber, 1.62 mg./cm.^{2}, was due to the mica window in the counter, and the air space between the sample and the window. The ratio of the activity with zero added absorber to the activity with zero total absorber, f_w, was determined to be 0.97.

Then from Eq. 39,

$$f_1 = \frac{m}{(A_\infty)\,(f_s)\,(f_w)}$$

$$= \frac{1774}{(25740)\,(1)\,(0.97)}$$

$$= 0.0712.$$

To determine f_w for the indium foils another absorption

curve was plotted on Figure 23. Since the indium foils decayed rapidly, it was necessary to normalize all activities to the net activity with zero absorber. The normalized activity was plotted versus absorber thickness on Figure 23. The value of f_w was calculated as it was for the thallium standard. It was determined to be 0.97. The values of f_w for thallium and indium were identical, but this was to be expected since the energies of the β particles are almost equal.

From the curve on Figure 23, the half thickness, $(\rho d)_{\frac{1}{2}}$, for the β of indium was determined to be 48.5 mg./cm.^{2}. The half thickness was determined by measuring the thickness of absorber needed to halve the activity. The absorption coefficient, μ_A, was calculated as follows (7, p. 198):

$$\mu_A = \frac{0.693}{(\rho d)_{\frac{1}{2}}} = \frac{0.693}{48.5} = 0.0143 \ \frac{\text{cm.}^2}{\text{mg.}} .$$

The self absorption factor, f_s, was then determined for the indium foils (2, p. 86),

$$f_s = \left[\frac{1}{(\mu_A)(t)} \right] \left[1-e^{-(\mu_A)(t)}\right] \qquad \text{Eq. 40}$$

$$= 0.6575,$$

where t = 63.6 mg./cm.^{2}, the thickness of the indium foil.

The actual saturation activity of the indium foils was determined from Eq. 39,

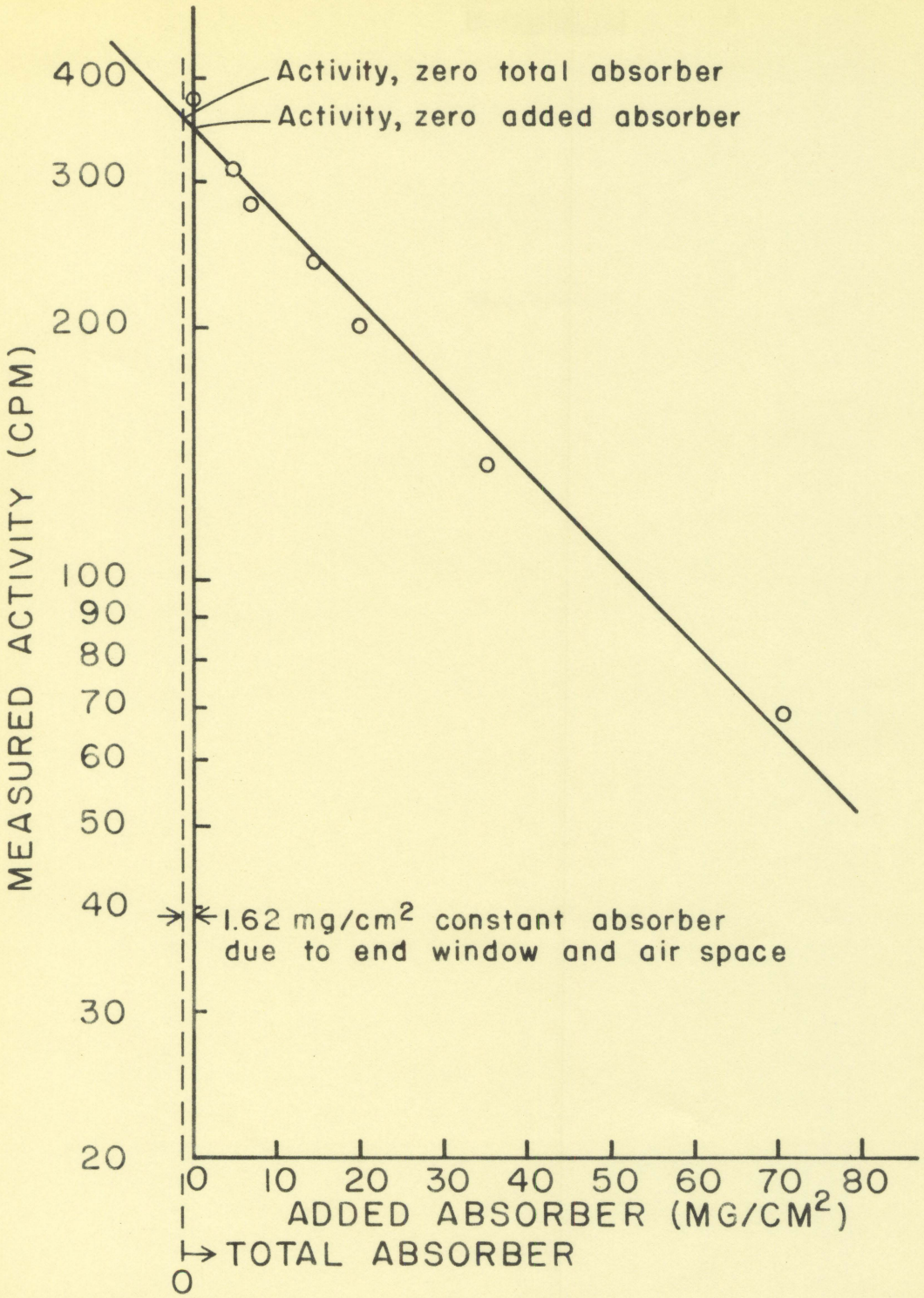

Figure 22. Thallium absorption curve

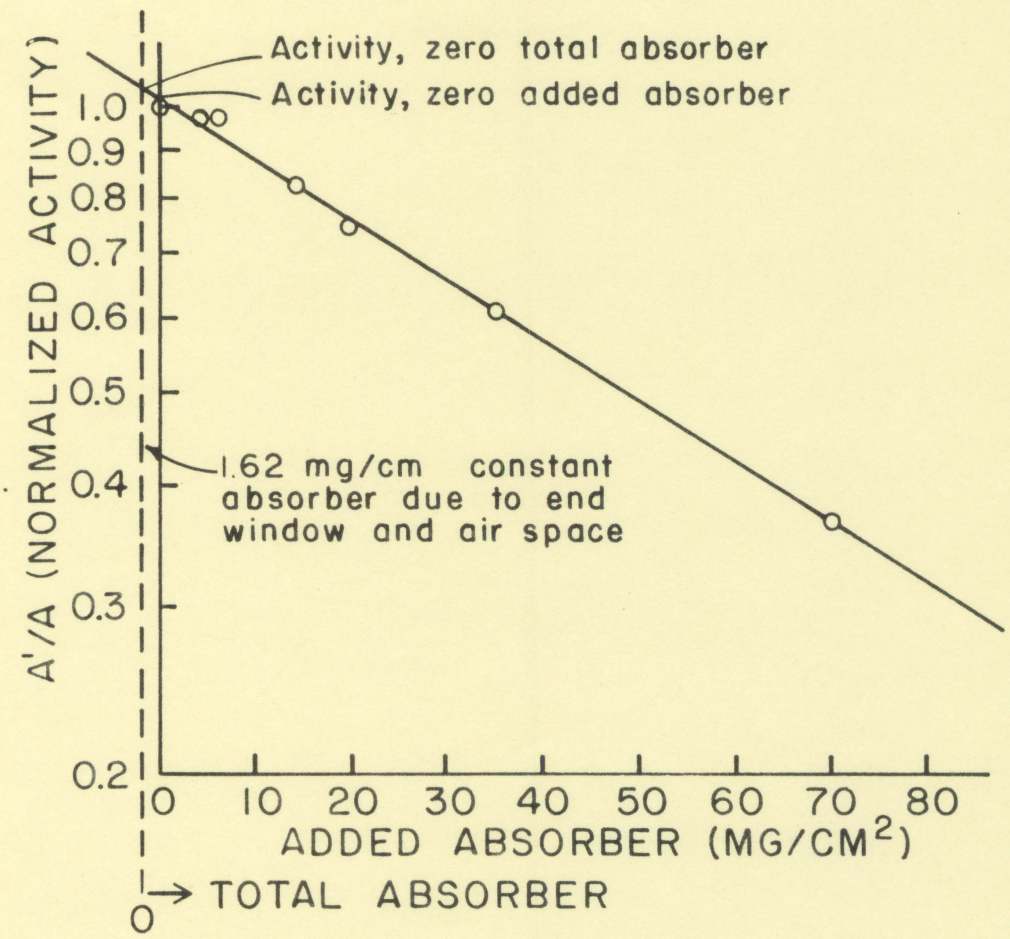

Figure 23. Indium absorption curve

$$A_\infty = \frac{m}{(f_1)\ (f_s)\ (f_w)}$$

$$= \frac{m}{(0.0712)\ (0.6575)\ (0.97)}$$

$$= \frac{m}{f_t} = \frac{m}{0.0454} \text{ cpm.}$$

The total correction factor, f_t, for all the indium foils counted was determined to be 0.0454.

APPENDIX B: MODERATOR CONSTANTS

General

The theoretical thermal flux distribution as developed in Eq. 14 of the text depended on the evaluation of constants pertaining to the geometry and the material of which the moderator was constructed.

Geometry Constants

Between the black boundaries, cadmium sheeting, the moderator measured 63.25 in. along the x axis, and 61 in. along the y axis. The extrapolated distance from the physical boundaries to zero flux was determined to be 0.75 in. by evaluating $0.71\lambda_t$ for pure graphite (6). This value agreed with the measured value obtained in Figure 4. Therefore, the distance between zero flux values along the x axis, a, was 64.75 in. The corresponding distance along the y axis, b, was 62.5 in. The distance between the source and zero flux along the z axis, c, was 79.75 in.

Determination of δ_{11}

For convenience, δ_{11} was calculated along the z axis with $x = y = 0$. The slope of the best straight line drawn through

the points on Figure 10 for x and y equal to zero was utilized as a trial value of γ_{11}.

The trial value of γ_{11} was used to calculate the end corrections,

$$C_e = 1 - e^{-2\gamma_{11}(c-z)}, \qquad \text{Eq. 41}$$

and the harmonic corrections,

$$C_h = 1 + \gamma_{11} e^{\gamma_{11} z} \left(\frac{e^{-\gamma_{13} z}}{\gamma_{13}} + \frac{e^{-\gamma_{31} z}}{\gamma_{31}} + \frac{e^{-\gamma_{33} z}}{\gamma_{33}}\right) \qquad \text{Eq. 42}$$

developed in Eq. 12. (The final values are tabulated in Table 4 for the correct value of γ_{11}). The various harmonic values of γ were calculated as follows (8, p. 121):

$$\gamma_{mn}^2 = \kappa^2 + \left(\frac{m\pi}{a}\right)^2 + \left(\frac{n\pi}{b}\right)^2 \qquad \text{Eq. 43}$$

$$\kappa^2 = \gamma_{11}^2 - \left(\frac{\pi}{a}\right)^2 - \left(\frac{\pi}{b}\right)^2 \qquad \text{Eq. 44}$$

The harmonic and end correction for each value of z were divided into the experimental value of ϕ to get ϕ_{11}. The values of ϕ_{11} from z = 24 in. to z = 54 in. were used to determine the value of γ_{11}. The values of z less than 24 in. were not used because of the effect of the fast neutrons at the lower level of the moderator. Values of z greater than 54 in. weren't used because the statistical deviation was high due to the decrease in flux, and also because of the change in lattice at this level.

Eq. 12,

$$\Phi_{11} = C\, e^{-\gamma_{11} z}, \qquad \text{Eq. 12}$$

was the type of equation which could be adapted to the determination of γ_{11} by the method of least squares (3, p. 166). The following procedure was used:

1. Tabulate the values of Φ_{11}, ln. Φ_{11}, z, z^2 and z ln. Φ_{11}.
2. Add the columns to get their summation.
3. Solve the following equations for γ_{11} and C where n is the number of values of z used in the procedure.

$$\Sigma \text{ ln.} \Phi_{11} = -\gamma_{11}(\Sigma z) + n \text{ (ln. } C). \qquad \text{Eq. 45}$$

$$\Sigma (z \text{ ln.} \Phi_{11}) = -\gamma_{11} (\Sigma z^2) + \text{ln. } C\ (\Sigma z). \qquad \text{Eq. 46}$$

The calculated value of γ_{11} was then used as a trial value, and the procedure was carried out again to calculate a better value of γ_{11}. The recalculation of γ_{11} was continued until the trial and calculated values were equal. This occurred at

$$\gamma_{11} = 0.085 \text{ in.}^{-1},$$

where

$$C = 48{,}985 \text{ neutrons/in.}^2 \text{ sec.}$$

$$= 7{,}593 \text{ neutrons/cm.}^2 \text{ sec.}$$

The diffusion coefficient, D, was assumed to be the coefficient for graphite, 0.356 in. (8, p. 127). The various

Table 5. Moderator constants

Constant	Value	
a	64.75	in.
b	62.50	in.
c	79.75	in.
γ_{11}	0.0850	$in.^{-1}$
χ	0.0485	$in.^{-1}$
γ_{13}	0.1660	$in.^{-1}$
γ_{31}	0.1618	$in.^{-1}$
γ_{33}	0.2155	$in.^{-1}$
C	$48.985(10)^3$	neutrons/ $cm.^2$ sec.
C	$7.593(10)^3$	neutrons/ $cm.^2$ sec.
D	0.356	in.

constants calculated in Appendix B are tabulated on Table 5.

APPENDIX C: STANDARD DEVIATION IN FLUX

To obtain the standard deviation in the neutron flux values, it was necessary to determine the coefficient of variation for each component affecting the flux. The coefficients of variation, C_v, are listed in Table 6.

Table 6. Coefficients of variation

Component	C_v
A_∞, thallium	0.050
f_s	0.050
f_w	0.020
σ_{act}	0.0322
A	0.004
N_a	0.00030
In^{115}/In	0.0010
f_c	0.050

The standard deviation, σ, is equal to the coefficient of variation multiplied by the component.

The value of f_1 determined from

$$f_1 = \frac{m}{A_\infty f_s f_w}, \qquad \text{Eq. 47}$$

was 0.0712. The standard deviation of f_1, σf_1, was obtained

from Eq. 48 (17, p. 207).

$$\frac{(\sigma f_1)^2}{(f_1)^2} = \frac{(\sigma_m)^2}{(m)^2} + \frac{(\sigma A_\infty)^2}{(A_\infty)^2} + \frac{(\sigma f_s)^2}{(f_s)^2} + \frac{(\sigma f_w)^2}{(f_w)^2} . \qquad \text{Eq. 48}$$

Eq. 48 is valid for the calculation of the standard deviation of products and quotients where the components are constant and independent of each other. The standard deviations of the components in Eq. 48 are listed in Table 7.

Table 7. Standard deviations

Component	Numerical evaluation	σ
m	1774.0	13.3
A_∞	25740.0	1285.0
f_s	1.00	0.050
f_w	0.97	0.194

From Eq. 48, σf_1 was determined to be 0.00540.

The value of f_t determined from Eq. 49,

$$f_t = f_1 \cdot f_s \cdot f_w, \qquad \text{Eq. 49}$$

was 0.0454. The standard deviation of f_t was obtained from Eq. 50.

$$\frac{(\sigma f_t)^2}{(f_t)^2} = \frac{(\sigma f_1)^2}{(f_1)^2} + \frac{(\sigma f_s)^2}{(f_s)^2} + \frac{(\sigma f_w)^2}{(f_w)^2} . \qquad \text{Eq. 50}$$

The standard deviations of the components in Eq. 50 are listed in Table 8.

Table 8. Standard deviations

Component	Numerical evaluation	σ
f_l	0.0712	0.00540
f_s	0.6575	0.03290
f_w	0.97	0.01940

From Eq. 50, σf_t was determined to be 0.004275.

The value of the neutron flux was determined from Eq. 29.

$$\Phi = \frac{m_w \; A \; f_c}{60 \; f_t \; \sigma_{act} \; N_a \; \frac{In^{115}}{in}} \; . \qquad \text{Eq. 29}$$

The standard deviations of the components in Eq. 29 are listed in Table 9.

Table 9. Standard deviations

Component	Numerical evaluation	σ
f_t	0.0454	$4.275\ (10)^{-3}$
σ_{act}	$155\ (10)^{-24}$	$5.000\ (10)^{-24}$
A	115	0.460
N_a	$6.023\ (10)^{23}$	$1.810\ (10)^{20}$

Table 9. (continued)

Component	Numerical evaluation	σ
In^{115}/In	0.9577	$9.577\ (10)^{-4}$
f_c	39/40	$4.880\ (10)^{-2}$

The standard deviation of Φ was obtained from Eq. 51.

$$\frac{(\sigma\Phi)^2}{(\Phi)^2} = \frac{(\sigma m_w)^2}{(m_w)^2} + \frac{(\sigma f_t)^2}{(f_t)^2} + \frac{(\sigma\sigma_{act})^2}{(\sigma_{act})^2} + \frac{(\sigma A)^2}{(A)^2} + \frac{(\sigma N_a)^2}{(N_a)^2} + \frac{(\sigma In^{115}/In)^2}{(In^{115}/In)^2} + \frac{(\sigma f_c)^2}{(f_c)^2} \qquad \text{Eq. 51}$$

$$= \frac{(\sigma m_w)^2}{(m_w)^2} + 0.01247.$$